Coastal mixing in multiple-mouth deltas: A case study in the Po delta, Italy

Article · June 2019

DOI: 10.1016/j.ecss.2019.106254

9 authors, including:

Debora Bellafiore
Italian National Research Council

Federica Braga
Italian National Research Council

Francesco Maicu
Italian National Research Council

Giuliano Lorenzetti
Italian National Research Council

Coastal mixing in multiple-mouth deltas: a case study in the Po Delta, Italy

Debora Bellafiore[a],*, Christian Ferrarin[a] , Federica Braga[a] , Luca Zaggia[c] , Francesco Maicu[a] , Giuliano Lorenzetti[a] , Giorgia Manfè[a] , Vittorio Brando[b] , Francesca De Pascalis[a]

[a] Institute of Marine Sciences- National Research Council (ISMAR-CNR), Castello 2737/F, 30122, Venice, Italy

[b]Institute of Marine Sciences- National Research Council (ISMAR-CNR),Via Fosso del Cavaliere 1, 00133, Rome, Italy

[c]Institute of Geosciences and Earth Resources - National Research Council (IGG-CNR), Via Gradenigo, 6, 35131, Padova, Italy

Abstract

Satellite imagery provides evidence of complex mixing dynamics in the coastal zone in front of multiple mouth deltas. One peculiar feature, identified in front of the Po Delta (Italy), consists in warmer water bulges present in some periods in the coastal zone between the river mouths. Such features are evident during both high and low river discharge.

Through an integrated approach based on the analysis of satellite imagery, in situ field data and a high-resolution oceanographic model, representing the whole river-delta-sea system, we investigated the relative contribution of the different forcing in controlling coastal mixing of riverine waters. The results evidence that the occurrence of these warmer saltier water bulges is due to upwelling induced by the combined action of tides and wind regimes aligned along coastline. Winds from the land and along the coast drive the upwelling through the well-known mechanism described by Ekman. The presence of river discharge enhance the water column stratification, creating the conditions in which tidal action follows the tidal straining theory. Both processes are identified in modeling results. The occurrence of these localized coastal waters with peculiar thermohaline characteristics, detectable on satellite imagery of the area, can be relevant in the definition of the freshwater areas of influence and the mechanisms of riverine water mixing in the near coastal zone. This can shed some light, eventually, on characterizing the sediment dynamics, as well as the thermohaline properties of waters in the area, and also to identify eventual impacts on the local ecosystems and fishery.

Keywords: Coastal mixing, Multiple-Mouth Delta, Satellite Imagery, Finite Element Model, Po Delta

*Corresponding author: Debora Bellafiore ISMAR-CNR, Castello 2737/D, 30122 Venice, Italy. Tel.: +39 041 2407936, Fax: +39 041 2407930
Email address: debora.bellafiore@ismar.cnr.it (Debora Bellafiore)

Preprint submitted to Estuarine Coastal and Shelf Science
November 23, 2018

Published paper can be found at
https://www.sciencedirect.com/science/article/pii/S0272771418309740
Embargo time 24 months

1. Introduction

The coastal area is characterised by complex dynamics between freshwater of continental

origin and salt waters. It shows a variety of transitional systems that can modulate the freshwater inputs into the sea. Deltas, estuaries and lagoons are also characterised by the presence of buoyant fluxes, sediment transport and a relatively fast morphological evolution.
Many studies focused on the classification of estuarine circulation (Hansen and Rattray, 1966; Garvine, 1995; Horner-Devine et al., 2015), providing tools for quantifying their main characteristics (Garvine, 1995; O' Donnell, 2010). The interaction between fresh and seawater leads to a number of hydrodynamic patterns, identifying water masses mechanically confined into a coherent shape close to the estuaries, with specific buoyancy, the so-called plumes. Their definitions and the capability to clearly state what are their borders are still subjects of discussion (Garvine, 1995; O' Donnell, 2010; Falcieri et al., 2014; Horner-Devine et al., 2015 and references therein) but their interaction with coastal waters explains part of the coastal mixing processes.
A certain part of river discharge is transported alongshore in downstream coastal current, while a part recirculates close to the river mouth creating an increasing area of buoyant waters, generally stabilised by tidal action (Fong and Geyer, 2002; Isobe, 2005, Chant et al., 2008).
In the comprehensive review by Horner-Devine et al. (2015), four different mixing areas within a river plume are identified: a) the river estuary as source region where strongly oriented forces prevail; b) the near-field where jets develop and momentum forces still prevail on buoyancy; c) the mid-field region where Coriolis force starts to dominate, diverting the plume to the coast; d) the far-field region that has no memory of the source, but the thermohaline characteristics of waters still allow to distinguish them from seawater. These four areas are the Regions Of Freshwater Influence - ROFI (Simpson et al., 1993). Along-shore wind forcing influences the development and extension of plumes, with different effects inversely proportional to the discharge rate: large river outflows (in the range 7600-31000 m^3s^{-1}, like for example the Rio de la Plata or the Yangtze River) produce plumes that are less subject to upwelling favourable winds and that rarely are destroyed by wind action. On the other hand, for small- or medium-range rivers, like the Delaware River or the Po River, subject of this work, wind action can eventually reverse and detach coastal currents and strongly affect river plumes (Pimenta et al., 2012). Wind forcing increase mixing along the plume, with major action just beyond the near-field (Hetland, 2005). A transition region is present between the near- and the middle-fields where offshore forcing prevail in propagating the plume signal, since shear mixing decreases. Moreover, the near- and middle-fields are the areas where rotational forces can counteract the plume spreading decreasing shear mixing (Cole and Hetland, 2016). Isobe (2005) clarifies that the ROFIs' characteristics are determined by the buoyancy-driven currents combined to the ambient currents.
Horner-Devine et al. (2015) reviewed mixing processes and the classification of coastal river plumes defining delta plumes as the ones that have regions of interaction due to the presence of multiple outlets. This configuration regards a large number of the major rivers worldwide, as the Mississippi River, the Nile and the larger Asian rivers (Wiseman and Garvine, 1995; Horner-Devine et al., 2015 and references therein).
Multiple buoyant fluxes can, therefore, develop and, if spatially close or enough energetic, they can interact laterally modulating coastal mixing. The area of interaction is strictly and geometrically linked to the velocity of the outflowing jet and the cross-section area of the river branch (Yuan and Horner-Devine, 2011). The interactions occurring between different rivers or multiple branches of the same river plumes were investigated also by Warrick et al. (2017). These authors describe how they can either collide or coalesce due to their thermohaline characteristics, the magnitude of river flow, their distance and the extent of their drainage basin.
Mixing processes occurring in coastal areas are of several types and respond to a number of additional factors: coastal currents are affected by the general hydrodynamics of the main basin and are modulated by local inputs, like rivers, lagoons and wetlands, modifying their

thermohaline characteristics and dynamics (Androulidakis et al., 2015). Moreover, on approaching the coast, from deep to shallow waters, mixing is also intensified by wave actions, which also have consequences on sediment resuspension (Karstner et al., 2018).
The morphology of the coast can contribute, with its complexity, in modifying the mixing dynamics. More generally, the interplay of marine hydrodynamics and riverine outflow affects sediment deposition shaping the delta area, identifying tides and waves as agents for sediment transport and morphologic evolution of the system (Leonardi et al., 2013, Leonardi et al., 2015, Maselli and Trincardi, 2013). In fact, the sediment deposition either within the core of the plume or along its lateral areas is dependent on sediment settling and eddy time scales (Mariotti et al., 2013).
Different portions of the coast can be affected by upwelling or downwelling, depending on wind regime and their orientation relative to the prevailing wind directions (Longdill et al., 2008). In fact, very local forcing, like winds, can be coupled to the larger-scale effects of other forcing, e.g. tides, that produce variations in the mixing rate in the water column, that is often linked to the characteristic time scales of the forcing (i.e. semi diurnal modification of the pycnocline that can be directly ascribed to the action of tides; Simpson and Souza 1995). In certain coastal areas, like ROFI, the interaction of stratified waters with tides originates the mixing process induced by tidal straining (Simpson et al., 1990; Simpson and Souza, 1995; Souza and Simpson, 1996; De Boer et al., 2009).
River plumes, modulating coastal exchange within the inner-shelf, play a role in transporting larvae, nutrients, sediments and pollutants in the open sea (Lentz and Fewings, 2012).
Spatially and temporally variable mixing processes, modulated by the main forcing and the complex coastal morphology can produce a number of small-scale structures that, despite their short lasting life, can affect the coastal hydrology and in turn the ecosystem.
For instance, coastal upwelling close to river mouths can trigger nutrient supply supporting phytoplankton blooms (Davis et al., 2014), increasing the potentials for fisheries.

In the present work we consider the mixing processes determined by the interaction of the plumes from multiple-mouth delta and coastal waters, evaluating how the different forcing affect dynamics in the mid-field plume and in the coastal areas between river mouths. As demonstrated in previous contributions by Brando et al. (2015) and Braga et al. (2017), the Po River prodelta is characterised by a complex dynamics of surficial waters, enhanced by the presence of the multiple branch system. The satellite images showed the presence of coastal areas between river mouths with turbidity values one order of magnitude lower than in the river plumes, though higher than in open sea waters, closer to those of marine waters.

This manuscript focus on these small scale near-shore water bulges located between different river mouths and having peculiar thermohaline characteristics. They can be detected from satellite, since their thermal signature differs from the near-field of the river plume. The occurrence of these isolated regions of water with different properties is not fully investigated and their genesis and evolution are still a subject of discussion. In this study, two interpretations are envisaged: a mechanism of horizontal entrapment due to the effect of multiple plumes isolating portions of seawater of the prodelta predating a discharge event, as originally postulated by Brando et al. (2015), or a mechanism of upwelling, very localized and linked to particular wind regimes and possible tidal action, in relation to the morphology and orientation of the delta coastlines.

1.1. Study Site

The Po is the largest Italian river: it originates in the western Alps and drains a large basin encompassed by the mountain ranges of the central and western Alps and northern Apennines. The catchment also comprises a vast and densely populated floodplain (Pianura Padana), for a total catchment area of about 74.000 km^2 representing a large proportion of the northern Italian territory. The river regime is characterized by periods of high runoff, due to either direct precipitation or snowmelt, generally in the fall or spring respectively, with maximum peak discharges reaching 10 000 m^3 s^{-1} and average discharge of about 1500 m^3 s^{-1} (Boldrin et al., 2005). Depending on the distribution of precipitation over the widely variable soils of the catchment, the river sediment load has a large variability and the trend of suspended sediment transport does not correspond to that of discharge magnitude and temporal evolution (Tesi et al., 2011).

The lower Po River originates a complex delta, with five main branches: Po di Maistra, Po di Pila, Po di Tolle, Po di Gnocca and Po di Goro (Fig. 1). Some secondary branches either flow directly into the sea or feed a system of seven coastal lagoons that characterize the delta: Caleri, Marinetta, Basson, Barbamarco, Canarin, Scardovari and Goro (Fig. 1). These are identified with different local terminology as, for example, palude or sacca.

The relative contribution of the distributaries, in terms of flow and sediment concentration and load can vary considerably in different regimes of river discharge (Braga et al., 2017; Maicu et al., 2018).

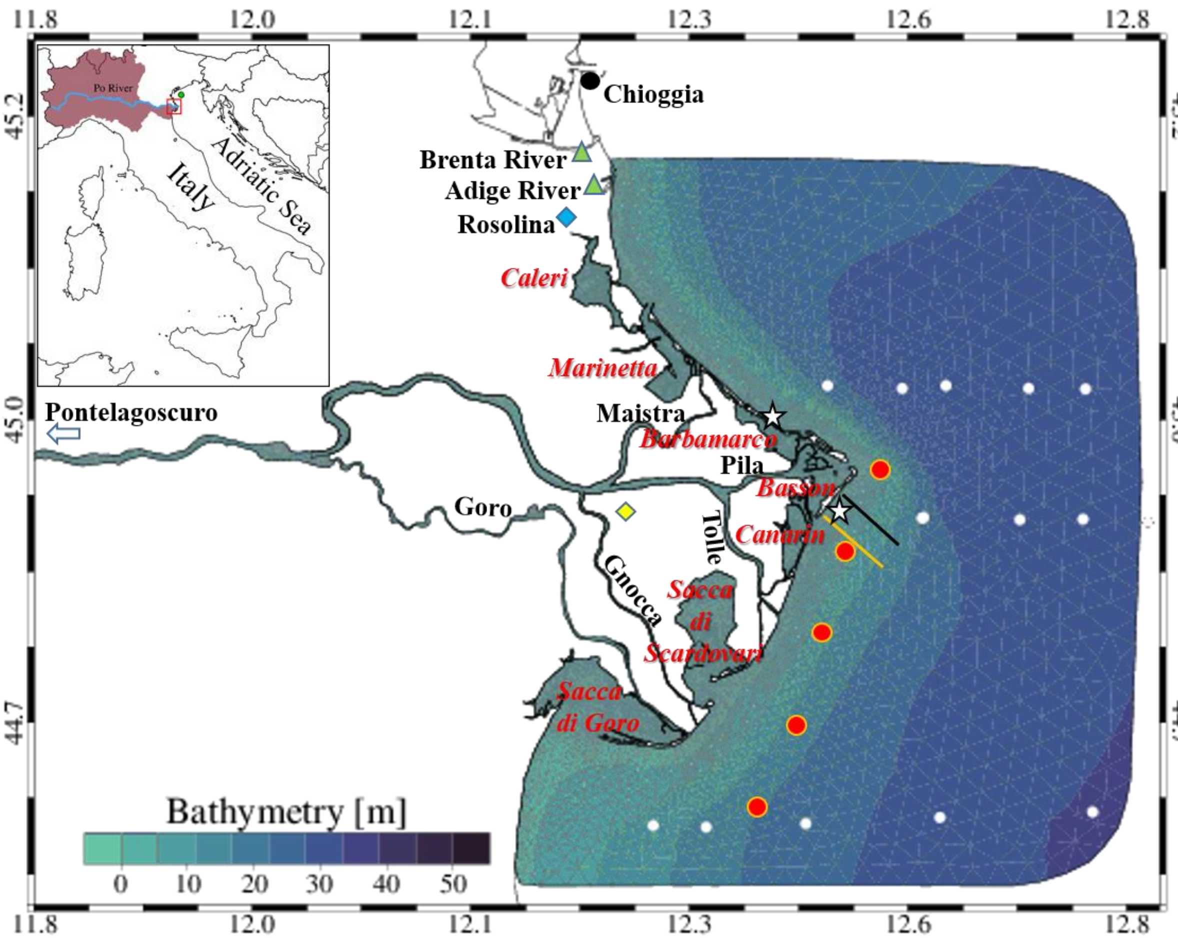

Figure 1: Computational grid and bathymetry of the study area: the Po River delta and adjacent coastal zone of the North Adriatic Sea. The geographic location of the study area (red box) in the North Adriatic Sea is shown in the upper left panel, where the green dot marks the CNR oceanographic platform. The yellow and light blue diamonds show the location of Po di Tolle and Rosolina meteo stations, while the black dot marks the tide gauge of Chioggia; the green triangles correspond to the location of the Brenta and Adige River mouths; the discharge gauge station of Pontelagoscuro is located 90 km upstream, as indicated by the blue arrow. CTD stations monitored during the RIT-PRODELTA oceanographic campaign are marked with: white dots for stations visited

by R/V G. Dallaporta and red dots for those visited by the Litus research boat. Transects considered for analysing modelling results for the events of the 19th November 2014 and 12th December 2014 are represented with black and yellow lines, respectively; white stars show the extraction points for analysed timeseries.

The Po river discharges into the North Adriatic Sea, a semi-enclosed basin connected to the Mediterranean Sea by the Otranto Strait. The Adriatic Sea has a shallow and gently sloping shelf, covering the full northern basin; the Po River prodelta reaches depths of about 20 m (Fig. 1). In this area, the general circulation on the Italian coast is characterized by a geostrophic coastal current, flowing from north to south (Artegiani et al., 1997a,b; Zavatarelli et al., 2002). This is modulated by the contribution of transitional water bodies (i.e. the Venice Lagoon, the Grado and Marano Lagoon) and river mouths (i.e. Isonzo, Tagliamento, Piave, Brenta, Adige and Po rivers, Bellafiore and Umgiesser 2010). The Adriatic Sea coastal circulation is driven by several forcing like meteomarine conditions (wind, atmospheric pressure, heat fluxes), tides and, as just mentioned, the buoyant fluxes from rivers. The main wind regimes characterizing the North Adriatic Sea and, specifically, the area in front of the Po River Delta, are Sirocco, from south-east and Bora, from northeast (Orlic et al., 1994). The Adriatic Sea is a micro-tidal environment, and the major tidal components are semidiurnal (M2, S2) and diurnal (K1) (Polli, 1960). The tidal signal is responsible for a water level range of 1 m, in spring tide conditions, in front of the Po Delta (Ferrarin et al., 2017).

2. Material and Methods

2.1. Satellite and in situ measurements

Several Landsat 8 thermal data were considered for the years 2013−2017 to identify the evidences of limited coastal areas, close and between the river mouths, that show different thermal characteristics from the surrounding waters. Landsat 8 platform carries two separate sensors: the Operational Land Imager (OLI) and the Thermal Infrared Radiometer Sensor (TIRS). OLI sensor provides coverage of the visible, near-infrared, and short-wave infrared portions of the spectrum at 30 m spatial resolution in nine spectral bands; the TIRS has two bands in the long-wave thermal infrared with spatial resolution of 100 m, resampled to 30 m (Irons et al., 2012). Landsat 8 images were obtained from the web resource USGS Earth Explorer (http://earthexplorer.usgs.gov/).

In total, five satellite images, acquired around 10:00 AM UTC, were selected in different river discharge conditions: the 19th November 2014, the 12th December 2014, the 29th November 2015, the 17th December 2016 and the 4th December 2017. To better understand and describe the process evolution, the Landsat 7 image acquired on the 18th of November 2014 was also used.

Sea Surface Temperature (SST) maps were retrieved from top-of-atmosphere brightness temperature (L_T) in the TIRS band 10 (10.9 m) applying the Eq. 1:

$$L_\lambda = (\tau \epsilon L_T) + (1-\varepsilon)L_d + L_u, \qquad (1)$$

where L_λ is the space-reaching radiance measured by the instrument, τ is the atmospheric transmission, ε is the water emissivity (0.98), L_d is the sky radiance (Barsi et al., 2005) and L_u is the atmospheric path radiance. LT was obtained converting the TIRS band 10 values to radiance values using the bias and gain values provided in the Landsat metadata file (Barsi et al., 2014). τ, L_u and L_d are specific to each individual scene and they were derived by the Atmospheric Correction Parameter Calculator (http://atmcorr.gsfc.nasa.gov/), which calculates the corresponding standard atmospheric profiles applying a MODTRAN radiative transferbased model (Barsi et al., 2005, 2014). The L_λ [W/(m^2 ster m)] to SST [◦ C] conversion was then performed using the Planck's Eq. 2

$$SST = \frac{K2}{ln\left(\frac{K1}{L_\lambda + 1}\right)} - 273.15, \qquad (2)$$

where K1 and K2, respectively the band-specific thermal conversion constants in W/(m^2 ster m) and in K.

It is worth mentioning that temperatures retrieved from Landsat 8 are normally higher than on site measurements, generally of about 1°C (Barsi et al., 2014; Martí-Cardona et al., 2019). Herein, TIRS data are used solely to detect relative SST differences between water bulges and plume waters due to current limitations in TIRS-derived SST accuracy and lack of in-situ skin temperature data.

Additionally, during the flood event of the 12th of December 2014 the RIT-PRODELTA joint oceanographic campaign was carried out in front of the Po Delta. Offshore sampling was performed on board of the research vessel G. Dallaporta while shallow coastal areas were investigated using the Litus research boat. Both vessels belong to the CNR research fleet. At each of the stations represented in Fig. 1, Conductivity-Temperature-Depth (CTD) profiles were acquired, with resolution about 10 cm, using Idronaut multi-parameter probes (Ocean Seven 316Plus and Ocean Seven 304Plus).

The CTD probes were also equipped with a turbidity sensor OBS (Optical Backscatter Sensor, Seapoint Turbidity Meter). Stations were selected to represent the whole range of variability of the prodelta waters: the more offshore stations characterize the seawater end-members while the alongshore transect allows the investigation of the border of the coastal area of interest. These latter and the southern East-West transect were visited on the 12th December 2014, between 7:20 and 11:00 UTC: they are considered almost synoptic and synchronous with the satellite overpass (9:58 UTC) and therefore adequate for SST validation (Donlon et al., 2002).

2.2. Numerical model description and simulation set-up

SHYFEM (Shallow water HYdrodynamic Finite Element Model (Umgiesser et al. (2014) and references therein), was applied for this study. It is a 3D finite element model, developed at CNR-ISMAR, based on the solution of primitive equations and previously applied on several transitional environments, coastal and shallow basins. It runs on unstructured staggered horizontal grids discretized in triangular elements of variable size. The vertical discretization can be either on zeta or sigma layers. The full description of the latest version of the code is provided in Bellafiore et al. (2018). The model has been recently applied to investigate hydrodynamics in the Po River-Sea System (RSS, Maicu et al. 2018).

For the present implementation, the model runs in the zeta layer configuration, with 20 vertical layers of increasing thickness, from 1 m in the topmost 10 layers, up to 4 m in the deepest ones. A constant bottom drag coefficient, set to 0.0025, is imposed. Heat and mass surface fluxes are parameterised according to the COARE (Coupled Ocean-Atmosphere Response Experiment) bulk formulae (Fairall et al., 2003). The system is forced with precipitation data from the Rosolina station, wind speed and direction from the Porto Tolle Station of the Regional Environmental Protection Agency of Veneto - ARPAV (Fig. 1). The other meteorological forcing (air temperature, cloud cover, relative humidity, solar radiation) come from data recorded by sensors on the CNR oceanographic platform "Acqua Alta" (Fig. 1). The choice to

use these latter datasets, instead of the measurements recorded in Porto Tolle Station, which is closest to the study area, comes from the fact that, being the Porto Tolle Station located on the land, the presence of land masses biases on these variables, registering colder air temperature not realistic for the sea state of the area studied.
The used grid covers the full Po Delta and the shelf in front of it, internal lagoons and the river up to Pontelagoscuro (90 km from the sea, Fig. 1). The bathymetric information interpolated on the grid is a merge of different sources: lagoons' bathymetry is from the land reclamation consortium "Consorzio di Bonifica Deltapo", except for the Goro lagoon whose bathymetry is provided by the Regional Environmental Protection Agency of Emilia Romagna (ARPAE). A CNR-ISMAR multibeam 2013 dataset, from RITMARE flagship project, provided Po di Pila bathymetry, while the internal branches are covered by dataset of the Po River Basin Management Agency (Agenzia Interregionale per il Fiume Po - AIPO).
The coastal bathymetry is a merge of data from NURC (NATO Undersea Research Centre), taken within the ADRIA 02 framework, and from CNR-ISMAR datasets in the North Adriatic Sea.
Two events were modelled, covering the periods 11^{th}–22^{th} November 2014 and 1^{st}–15^{th} December 2014. The model implementations get initial conditions for water level, velocity, temperature and salinity from a longer reference run starting the 1^{st} of November 2014.
Boundary conditions for water levels, 3D currents, temperature and salinity are from the operational model TIRESIA of the whole Adriatic Sea (Ferrarin et al., 2019). Po River discharge and temperature are imposed at the open boundaries at the distributaries from ARPAE monitoring station, in Pontelagoscuro. For the Adige River, while the discharge is that measured by ARPAV, the water temperature has been set equal to 2° C less than that of the Po River. This latter assumption is deduced from data of the SST imagery of the 19^{th} of November 2014 in Brando et al. (2015).

In order to proceed with the process investigation, a simulation protocol was defined, based on quantifying the effects of the major forcing. For each event three simulation runs were performed: the first used the full set of forcing and is called ALL run; in the second, called NO TIDE run, the boundary condition time series were filtered for tides through a simple moving average with a 2 days window. Therefore, the system is laterally forced at the sea boundary only by the surge signal, with corresponding temperature and salinity variations; the last, called NO WIND run, imposed tides and the heat and mass fluxes but the wind forcing was not imposed.

3. Results

3.1. Earth observation and in situ measurement evidences

All the five selected Landsat 8 images are characterised by the occurrence of small near-shore water bulges, which are warmer than the adjacent plumes and the coastal current, with values similar to those of the central part of the basin. These water bulges are located in the areas between the distributary mouths. Despite the intrinsic noise affecting the Landsat 7 sensor, the image acquired on the 18th of November 2014, the day before the Landsat 8 acquisition described in Brando et al. (2015), is also considered as it shows more evidently the warmer near-shore water parcels. These events are here analysed considering the corresponding SST maps and correlating evidences with information on the river flow and the trend of meteomarine forcing (wind, tidal phase) shown in Table 1.

Table 1: Meteomarine conditions and river discharge data corresponding to the selected events,

which are characterized by the occurrence of small warmer near-shore water parcels. Tide data from Chioggia Diga Sud (ISPRA); tidal phase: E=Ebb, F= Flood, EF= Ebb to Flood, FE= Flood to Ebb. Wind data from Porto Tolle meteorological station (ARPAV); wind speed range is for the 12 hours before the event. Po river daily mean discharge from Pontelagoscuro gauge station (ARPAE).

Event	River Discharge [$m^3 s^{-1}$]	Differences River-Sea SST [◦C]	Wind Direction (Provenience)	Wind Speed [ms^{-1}]	Water Level Range [m]	Tidal Phase
18/11/2014	8531	-3.4	NW - W	2.1-6.6	0.90	FE
19/11/2014	8603	-3.3	NW - W	0.5-2.8	0.70	FE
12/12/2014	2748	-4.8	SW -W	0.9-1.9	0.30	EF
29/11/2015	914	-5.5	W	0.3-1.9	0.95	EF
17/12/2016	1101	-6	NW - W	1.2-2.3	0.85	EF
4/12/2017	674	-5.8	NW - W	1.2-1.9	1.30	F

The considered events are all fall/winter phenomena, with riverine water temperature always colder than the sea water (ΔSST from 3 to 6°C). The 18 − 19th November 2014 and the 12th December 2014 events correspond to high and medium/high discharges, while the others are in low discharge conditions. In all cases, weak winds from the land with slightly variable direction were recorded: generally from NW-W, with the exception of the 12th of December 2014, when direction was SW-W. The satellite passed in different tidal phases, generally in the transient between high (flood) and low (ebb) water level or viceversa, when there are the highest tidal currents normally occur. Only the 4th of December 2017 is in fully flood phase.

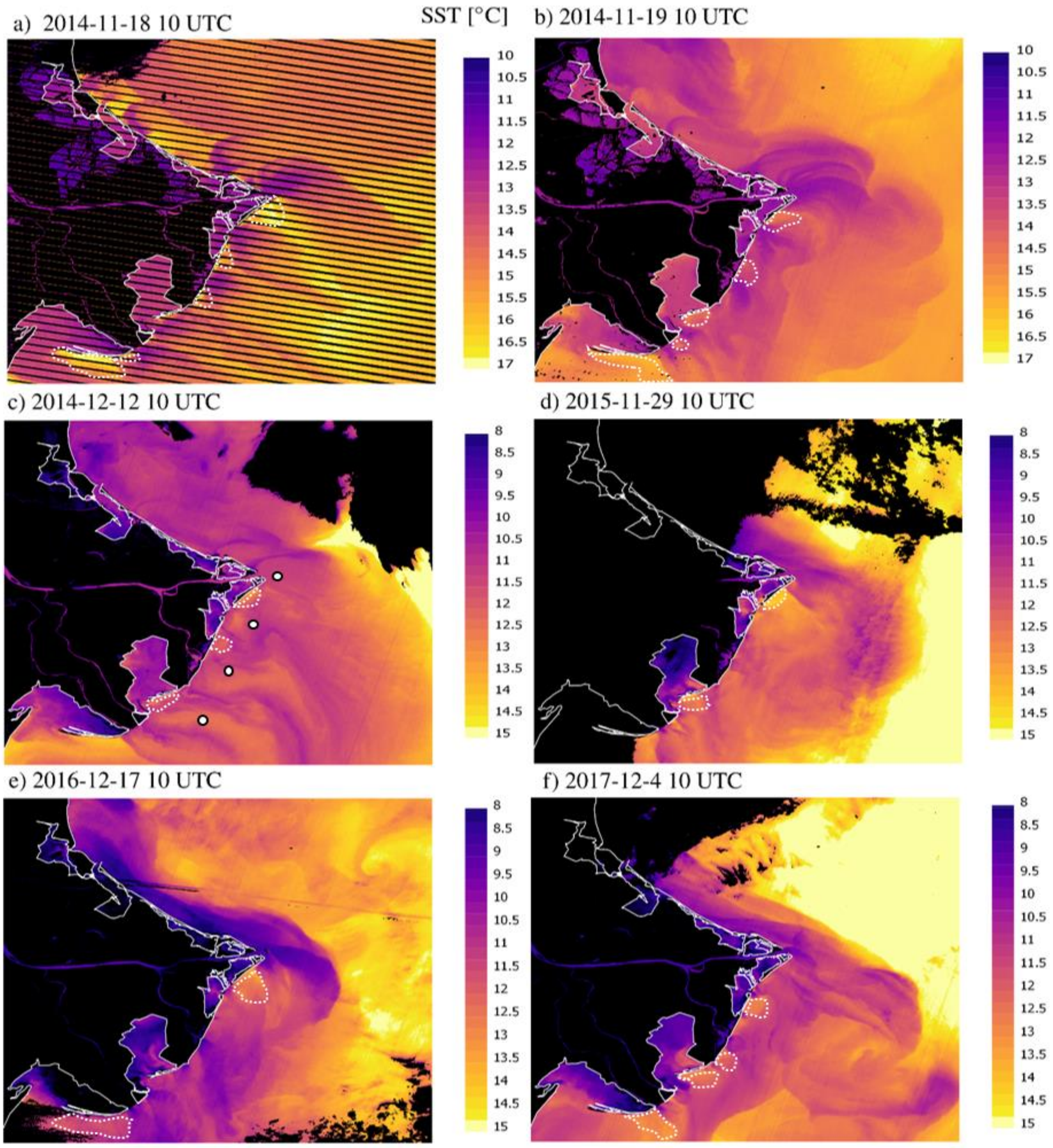

Figure 2: SST maps from Landsat 7 and Landsat 8 TIRS: a) 18th November 2014, b) 19th November 2014, c) 12th December 2014 (white dots represent the Litus CTD casts), d) 29th November 2015, e) 17th December 2016 and f) 4th December 2017 (about 10:00 UTC). Limited coastal areas, indicated with white dotted closed lines, between the river mouths, show thermal characteristics closer to marine waters.

On the 18th–19th November 2014, the SST maps from Landsat 7 and Landsat 8 TIRS show a number of near-shore warmer water bulges: along the northern and southern parts of the Po Delta coast on the 18th of November; mainly on the southern part below the Pila mouth and between the river mouths, on the 19th of November (Fig. 2,a and b). Their shapes are thermally more evident from the Landsat 7 image, with areas even warmer than 17° C. The observed thermal characteristics suggest that their origin could be marine, rather than continental, even if it is not possible to clearly state from satellite images whether these waters were entrapped just superficially by the multiple river plumes or their thermal characteristics are detected also below the surface, suggesting possible upwelling. For both SST maps, a quite large area along the sandbar bordering Sacca di Goro also shows thermal values closer to those of offshore waters (Fig. 2a and b). River waters are also easily traced by the high discharge associated to this event. Fig. 2 a and b clearly shows the jet of each distributary forming cold plumes with initial seaward trajectories that are deflected south by the Coriolis force and the potential vorticity conservation. The satellite-derived SST of the 19th of November 2014, compared to the previous one, shows that the extent of the plumes and the spreading of colder riverine waters cover a wider area. The two images are both in correspondence with the flood to ebb tidal phase. Interestingly, the internal boundary of both Sacca di Goro and Sacca di Scardovari is characterised by warmer water compared to the surrounding areas (15 vs. 13° C).

On the 12th of December 2014, the SST image identifies one bulge of warmer waters between the Pila and Tolle mouths and two thin fringes of waters around 16° C in front of the sandy bar that separates the Sacca di Scardovari from the sea (Fig. 2c). Warmer waters (> 14.5° C) are present, as well, along the coast in front of Sacca di Goro. The fronts of the cold river plumes are less marked compared to the thermal tracer of marine waters, but still distinguishable, due to the lower discharge, compared to the 18th–19th November 2014. The shape of warm water bulges, more compressed along the coast, could be affected by the tidal force to the coast typical of the semidiurnal component of tides, in the ebb to flood phase. The other three events are all characterized by low discharge: on the 29th of November 2015 the presence of the warm water bulge at south of the Pila mouth is visible as a localised coastal spot with temperature > 14° C (Fig. 2d), surrounded by colder waters (13° C) but not as cold as the river waters (10° C, Fig. 2 d and Table 1). This low-discharge event does not convey enough freshwater into the system to significantly affect the area at south of the Pila mouth. For this event, as well as the events of the 17th of December 2016 and the 4th of December 2017, both associated to low discharge (Fig. 2 e and f), also the contribution of the Brenta and Adige rivers, located at north of the Po delta, plays a fundamental role. They form an almost 1 km large band of colder water along the northern coast of the delta and eventually produce a southward coastal current that dominates the dynamics of the area.

This feature does not affect the southern part of the delta, where the warmer water bulges are in any case observable during the 17th of December 2016 and the 4th of December 2017.

Simultaneously to the satellite overpass on the 12th December 2014, in situ data were collected (Fig. 3, left panels for location and surface values).

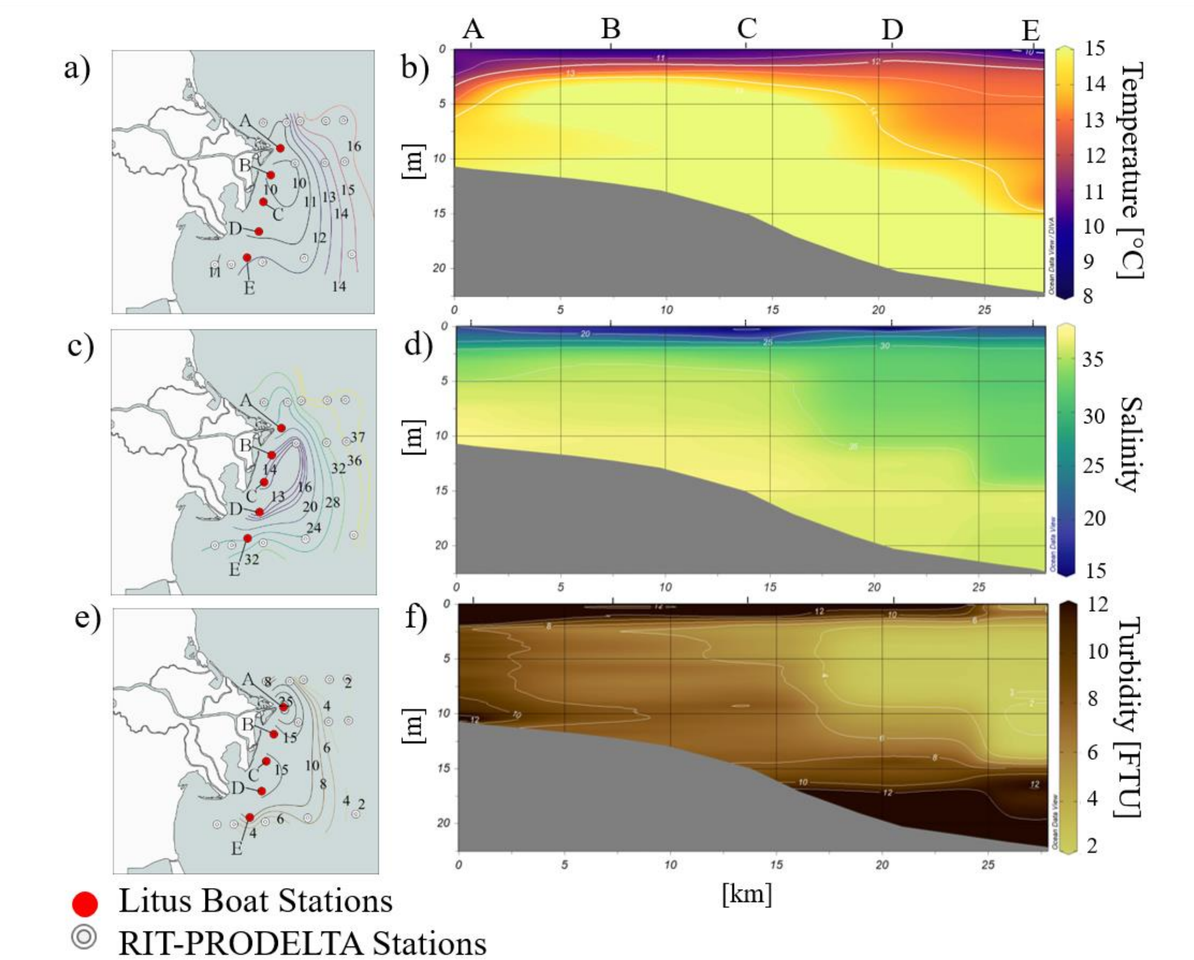

Figure 3: Field measurements, on the 12th December 2014. Left, a, c and e) Surface maps of measured temperature, salinity and turbidity. Right, b, d and f) Transect of LITUS profiles (temperature, salinity and turbidity) along coast from north to south (red dots in the left panels).

The CTD casts (shown as red dots in Fig. 3), although acquired slightly more offshore than the area where warmer water coastal bulges are observed, can provide useful information about temperature, salinity and turbidity distributions, potentially connected to the investigated mixing processes in the prodelta. The presence of the freshwater buoyant plume is evident at the surface, particularly on the southern coast of the delta. CTD profiles show a strong stratification with colder, fresher and more turbid waters at the surface, and a sharp gradient located at 2-3 m; this gradient reduces moving south to the stations D and E.

Considering the temperature and salinity pattern from CTD casts, no clear evidence of warmer water bulge can be detected at the surface (Fig. 3a and c). However, the analysis of the along-coast transect from LITUS casts in the coastal area south of Pila (stations B and C) reveals the presence of a warmer (temperature more than 15°C) and saltier (salinity is higher than 35) structure at depths between 3 and 7 m (fig. 3b and d). We interpret this as an intrusion of offshore water in the mid layer close to the coast. This structure compresses the buoyant plume, giving rise to the formation of the sharp gradient observed between stations B and C. As a consequence, the vertical profiles outside the area of the described structure show a higher degree of mixing, with a deepening of the layer with salinity lower than 35 to 5 m, in front of the Pila mouth (station A), and to 12 m, in the southern part of the delta close to the Sacca di Goro (station E). A higher degree of stratification with lower salinity, in the very surficial waters, is visible south of Po di Tolle mouth (station C). In particular, the CTD station between the river mouths of Pila and Tolle (station B) shows a thinner surface layer of fresher and colder water, compared to the surrounding, which is accompanied by a slight decrease in turbidity (Fig. 3b, d and f).

The stations closer to the Po River distributaries show higher values of turbidity on the surface, particularly in front of the Pila mouth (station A, Fig. 3). Turbidity is progressively decreased from A going south and there is a small decrease of turbidity, at stations B and C, at around 8 m depth (5-6 FTU). Therefore, we hypothesize that the water characterizing the warmer and saltier water area at mid depth (stations B and C) could have origin from offshore or at least been mixed with it.

3.2. Model Validation

Two of the above-mentioned events, the ones where both the phenomenon is clearly visible and there is the availability of data to force and to validate results, are reproduced by the model. The 19th of November 2014 is compared to satellite images, while the 12th of December 2014 is validated also against CTD casts. Once the robustness of the proposed tool is verified, it can then be used to investigate the full process, for those specific events and eventually for others. Fig. 4 shows the difference between model results and satellite data, for the two events.

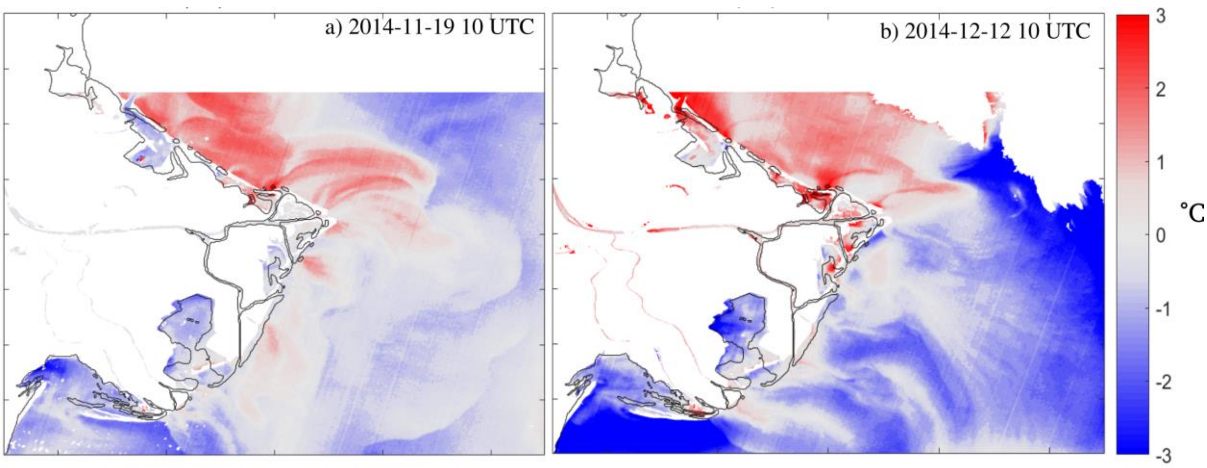

Figure 4: Model - surface temperature difference for the event of a) the 19th November 2014 and b) the 12th December 2014.

For the day 19th of November 2014, Fig. 4 indicates how surface temperature offshore is slightly colder than the one detected by the satellite but within the 1°C error. This value is considered acceptable, as discussed in Donlon et al. (2002), because we are comparing the satellite measured skin temperature that can differ, due to thermal stratification, from the sea surface temperature computed by the model at 0.5 m depth. The major discrepancy between modelled and measured data are seen in the northernmost coastal area of the Po Delta, with a model overestimation of about 2°C. It is reasonable to think that a certain influence of the discharge of the Adige River, located at north, can be the cause, due to the lack of direct temperature measurements and with the imposition, as forcing, of the same temperature timeseries used for the Po River, reduced of about 2°C that can lead to a certain mismatch. However, the full areas of the near- and far-field of the Po River plume seem to be well reproduced, with a large range of difference below 0.5°C. Since this value is well below the river-open sea temperature gradient, we consider that the model performance in the areas where warmer and saltier water bulges appear are acceptable.

For the event of the 12th of December 2014 (Fig. 4, right panel), the model reproduces a colder marine environment, compared to the image. Error patterns are similar, even if higher in value, compared to the first simulated event. As an average over the studied area, the model underestimates the SST recorded by the satellite of about 0.3°C. The negative bias in the offshore area could be partially ascribed to the used surface heat forcing used that are taken from CNR platform. Being this station located north of the simulated area, surface fluxes, even if more realistic than other datasets (for instance the Porto Tolle Station that, being located inland, does not measure the correct sea-air exchange), can be slightly biased. Moreover, taking advantage from the CTD dataset acquired simultaneously to the satellite overpass, we can estimate whether the discrepancy is fully ascribable to the model performances or a systematic error is associated to the satellite imagery.

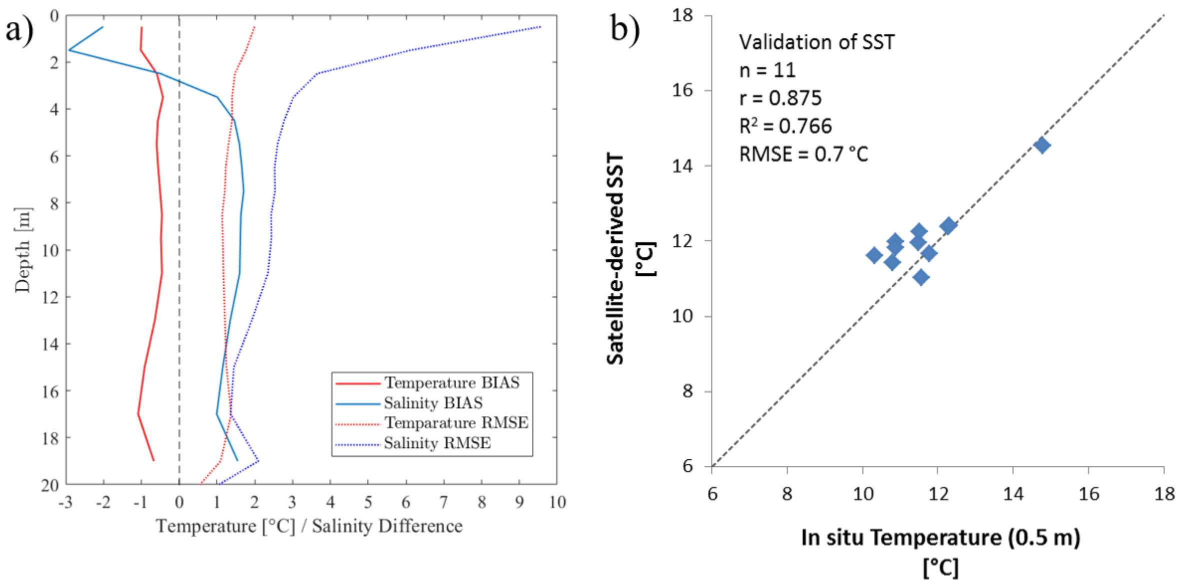

Figure 5: a) Model and CTD comparison for the field campaign of the 12th December 2014. Data from model are extracted in the correspondence of each CTD cast. Temperature (red) and salinity (blue) Bias (plain line) and RMSE (dotted line); b) Scatter plot of satellite-derived SST and in situ temperature from CTD casts (mean value of the upper 0.5-m) in 11 stations. The statistics of fitting are given as correlation coefficient (r), coefficient of determination (R2), relative root means square error (RMSE). The 1:1 line is plotted as dotted lines.

Fig. 5a shows temperature and salinity biases and root mean square errors (RMSE), when comparing modelled profiles and CTD casts. Results are encouraging, with a negative, almost constant, model temperature bias of less than 1°C. Temperature RMSE is lower than +2°C on the surface and lower than 1°C over the water column, detecting the small thermal gradient that characterises the event. From the comparison it is evident how the model performances are similar vertically, an encouraging aspect to state the model robustness in the reproduction of the full 3D process. Salinity bias is −2 on the surface, while it is around 1 on the water column. Being the haline gradient in the area reaching more than 30, a discrepancy of few units should be considered an acceptable result. The highest salinity RMSE is, as expected, on the surface (9 units) due to the large range of salinity values in the studied area, going from riverine environment to marine one in few kilometres.

Considering the in situ measurements as the closest to reality, we have also a verification of the SST data quality: the satellite-derived data against in-situ data validation is shown in Fig. 5b. The mean satellite-derived SST error (RMSE) calculated on the basis of bulk temperature from CTD data is about +0.7 °C. As demonstrated by Brando et al. (2015) and Manzo et al. (2018), Landsat-8 data was able to capture and support the investigation of the Po River prodelta in correlation with hydrometereological data at the submesoscale. However, it is worth mentioning that temperatures retrieved from Landsat 8 are normally higher than on site measurements, as well confirmed in this study. This finding is consistent with other studies which found a systematic overestimation of Landsat 8 temperatures (Barsi et al., 2014; Martí-Cardona et al., 2019).

3.3. Sensitivity tests on dominant forces

In order to evaluate the process driving the formation of the warmer bulges, we performed two sets of simulations, for both events on the 19th of November 2014 and 12th of December 2014. The first group of runs considered the full set of forcing and, as presented in the previous section, were the ones compared to measurements (ALL runs). A process-based strategy was then adopted to investigate the major drivers responsible for the warmer bulges formation: modelling results of previous test, not shown here, where heat and mass surface fluxes were switched off, demonstrated the minimal influence of this factor for the studied events. Given the fact that both cases correspond to flood events, even if of different entities, we investigated the effects of tides and wind action, filtering out the former (NO TIDE runs) or switching off the latter (NO WIND runs). Simulated surface temperature and salinity, in the three runs, for the snapshot in correspondence with the satellite overpass are shown in Fig. 6, for the days 19^{th} of November 2014 and in Fig. 7, for the day 12^{th} of December 2014.

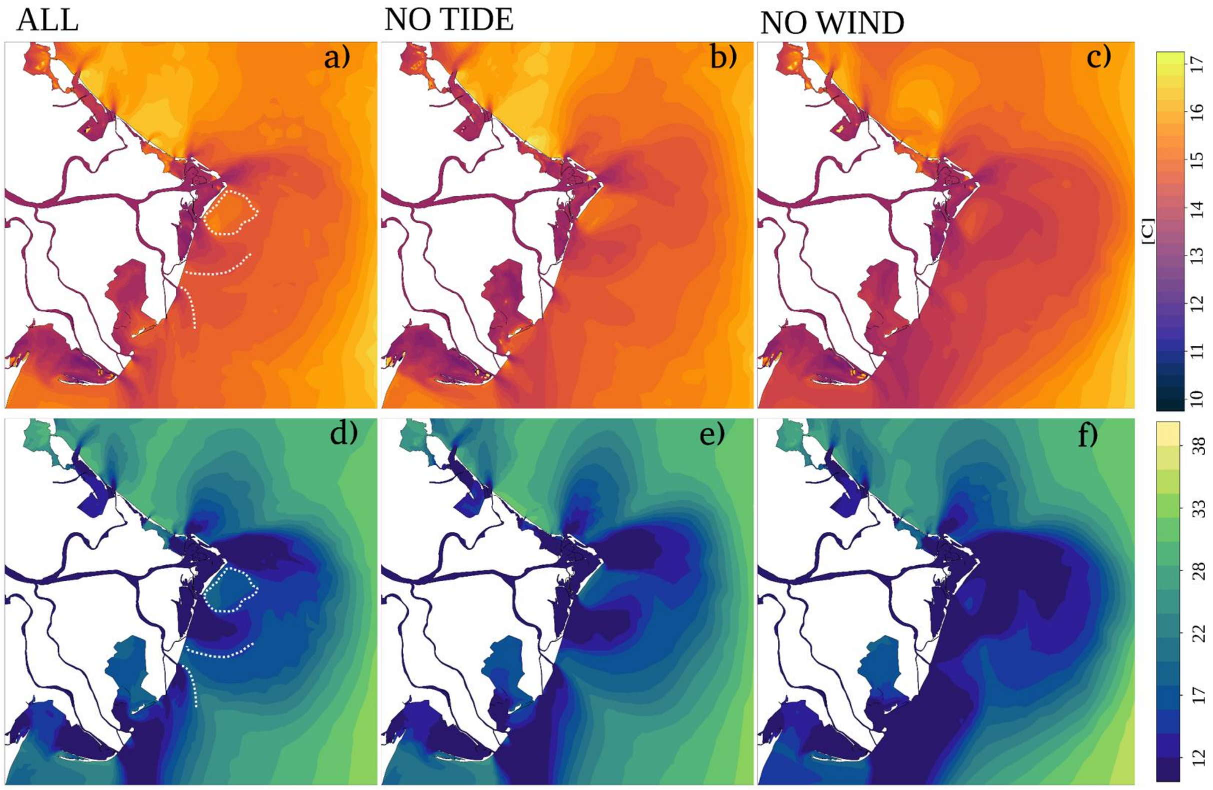

Figure 6: Surficial temperature (a, b, c) and salinity (d, e, f) maps for the run fully forced (ALL), the run without tide forcing (NO TIDE) and the run without wind forcing (NO WIND), 19^{th} of November 2014. White dotted lines in a) and d) show the different nature of process, identifying enclosed surface warmer and saltier waters south of Pila mouth, while just the borders of different plumes are seen in front of Po di Tolle mouth.

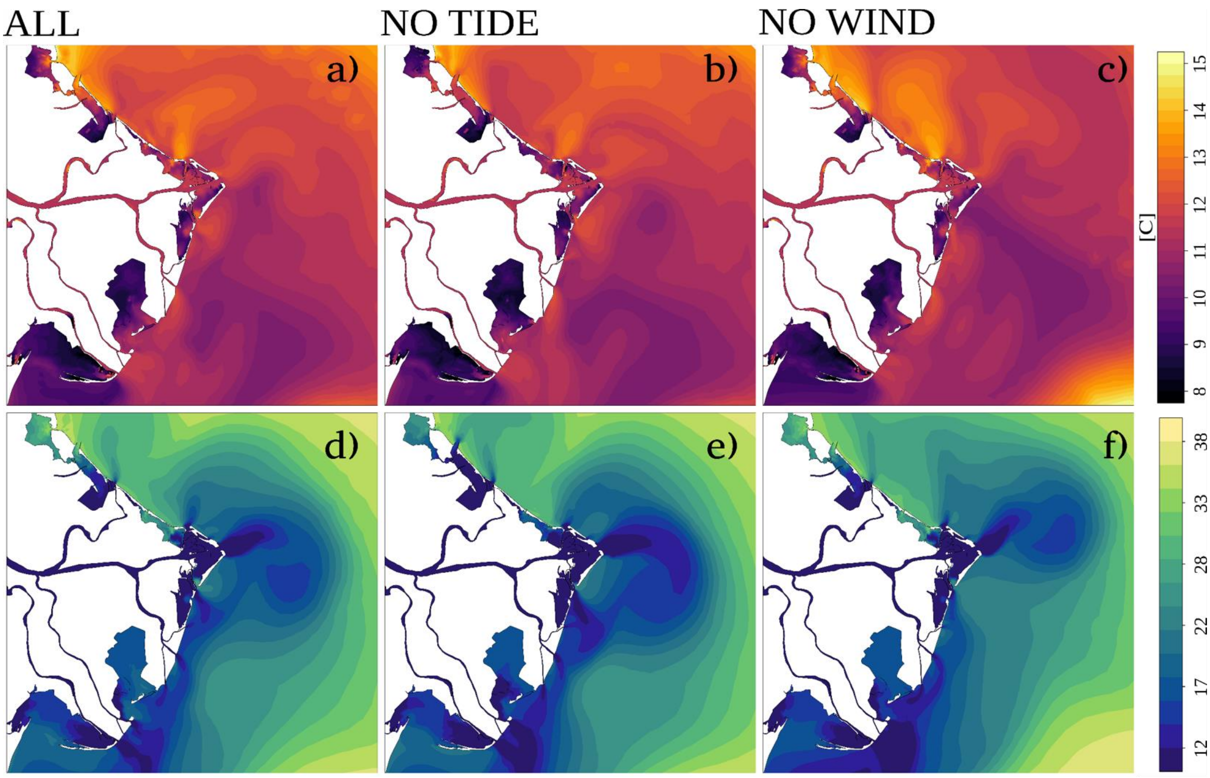

Figure 7: Surficial temperature (a, b, c) and salinity (d, e, f) maps for the run fully forced (ALL), the run without tide forcing (NO TIDE) and the run without wind forcing (NO WIND), 12th of December 2014.

Moreover, salinity and temperature cross-shore transects (see Fig. 1 for locations), through the areas where the warmer bulges are seen, are extracted for the three runs for each event (Fig. 8). The location of the transects in the two dates differs of about 2 km, as they were centred on the warmer water bulge on each SST image.

On the 19th of November 2014, the warmer water bulge south of the Pila mouth is seen (12.5°C), surrounded by riverine water. The bulge just south, close to Po di Tolle mouths is less evident in temperature (14.5°C), but still present (Fig. 6 a and d, white closed dotted lines). Salinity signature clearly shows higher values in a detached area south of Pila mouth, bordered by lower salinity waters. On the other hand in front of the Po di Tolle mouth, with its three inlets, just the plumes borders can be detected. This suggests that the typologies of process occurring south of Po di Pila and close to Po di Tolle are different, inferring that the former can be a point of upwelling, while the latter represents entrapped (or more correctly, bounded) marine waters between plumes (Fig. 6 a and d, white lines help in identifying the area).

Once tides are filtered out from the water level boundary condition, the surface patterns, both in temperature and in salinity, still present warmer and saltier bulges, not completely differing from the results of the fully forced run. However, some variations can be seen, specifically in the extension of the colder and fresher water signal of the river plumes offshore that is increased in absence of tides (Figs. 6b and e). The bulge of higher salinity between the Pila and northern Tolle mouths is more adherent to the coast in the NO TIDE run, while the other surface patterns detected in the ALL run are still present and not significantly modified. Therefore, from the evidences arising from the surface patterns, a possible effect of tides in modulating the dynamics has to be considered, even if tides do not completely modify the phenomenon in this event.

On the other hand, once tides are reintroduced and surface wind excluded, the surface temperature and salinity patterns change significantly, with the almost total disappearance of the warmer saltier water bulges (Figs. 6, c and f panels). As an average, the full coastal zone south of the Pila mouth seems colder and fresher than in the corresponding ALL run; there is

a weak signature of a warmer bulge just south of Pila but the gradient with the surrounding water is lower (less than 1°C vs. more than 2°C in the ALL run). In salinity, the area where the marine water bulge is expected shows waters with salinity values not higher than 17.
The extracted transect shows, if tides are not imposed, a weak signal in salinity (20 vs. 17) with a water column slightly less stratified than the ALL run (Fig. 8d and e).

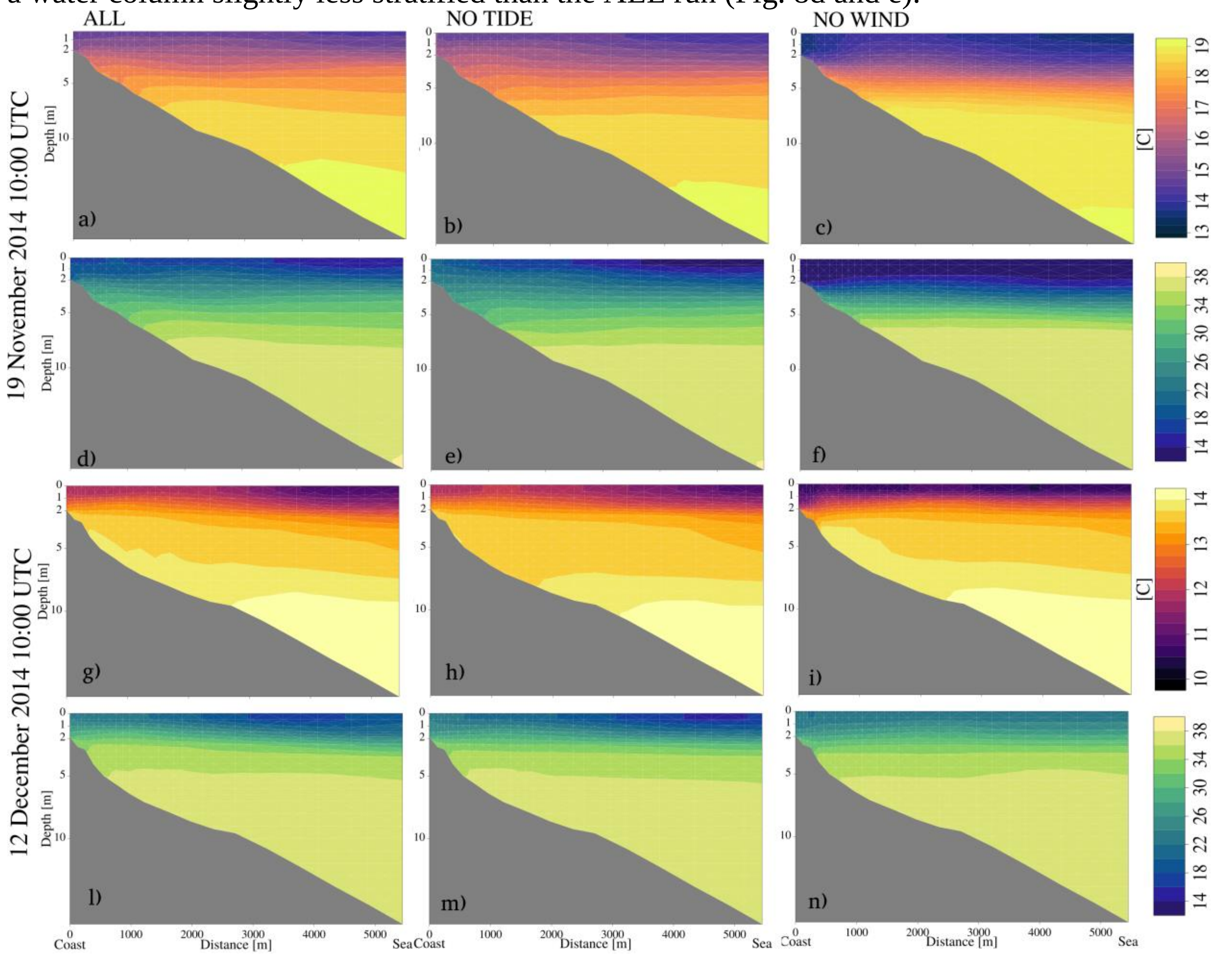

Figure 8: Temperature (a,b,c,g,h,i panels) and salinity (d,e,f,l,m,n panels) transects in the study area (black and yellow line in Fig.1) for the three simulations on the 19th of November 2014, 10:00 UTC (top panels) and on the 12th of December 2014, 10:00 UTC (bottom panels). Note the differences in temperature and salinity ranges between the dates.

The absence of wind, on the other hand, drives fresher and colder water on the surface, opposing to possible upwelling. The NO WIND run seems to reproduce a more vertically stratified coastal environment because of the occurrence of a major river flood. In fact, the energy injected into the system by the river, in the absence of wind forcing, seems to fully dominate the coastal dynamics (Fig. 6c and f).
The simulation of the event of the 12th of December 2014 with the full set of forcing shows how the river mouths inject almost similar waters in temperature compared to the surroundings (13° C vs. 12° C, Fig. 7a). The presence of waters with different characteristics is more evident in the surface salinity snapshot, where areas are detected, along the delta, south of the Pila mouth, with salinity higher than 30 (Fig. 7d). The largest bulge is the one just south of Pila, followed by a small one just north of Po di Tolle mouth. The third structure forms between the multiple ramification of the Po di Tolle mouth. Interestingly, the same thermohaline characteristics of the bulge are seen in some parts of the coastal lagoon (Caleri), suggesting the possible influence of these processes on lagoons' internal characteristics.
Finally, a quite large area with higher salinity close to coast can be seen in front of the Goro

Lagoon. In our simulation this latter bulge seems to be detectable just in salinity, with cold waters in the full area both inside and outside the Goro Lagoon. However, from the SST image in Fig. 2b, that one seems a warmer area, at least along the coastal area. If tidal forcing is not applied, the pattern both in temperature and in salinity does not change significantly in shape, even if the area where warmer and saltier waters can be detected is larger 7b and e). The shape of the low salinity plume at the Pila mouth keeps its coherence and its boundaries are clearly visible and deflecting to south. Finally, the absence of the wind forcing leads to the disappearance of the bounded area of higher salinity (Fig. 7f), both south of Pila and in front of Goro Lagoon. This aspect also applies to the temperature fields.
Looking at the extracted cross-shore transect, if tides are not considered, the warmer tongue (around 14° C), detected at the bottom close to the coast ($4 - 5$ m depth) in the ALL run, is maintained more offshore (at 10 m depth, Fig. 8g and h). The same behaviour is not as evident in salinity but, due to earth rotation and absence of tides, the far-field action on the river plume can push fresher surface water in the area. Excluding wind forcing, surface waters are cooler and saltier (Fig. 7). However, the warmer bottom tongue reaches shallower areas, as in the ALL run (Fig. 8i and n). Therefore, it seems that both forcing, with different mechanisms, like the action of tides on the bottom layer in intruding warmer water and the action of wind in pushing coastal warmer waters offshore, contribute to the formation and shaping of the bulge.

4. Discussion

The starting point of our investigation were the satellite-derived SST maps that show how warmer water bulges appear in several areas along the coast, always between the river distributaries and are thermally more visible in the fall/winter season (Fig. 2). The modelling tool, used to perform sensitivity analysis and to infer on the process genesis and evolution, is complementing the information, clarifying how these patterns are also characterized by water saltier than the surrounding (Figs. 6 and 7).

A first consideration is linked to the morphological complexity of deltaic systems. The Po River Delta shows a complex coastline that varies orientation over a range of few kilometres. Despite a general homogeneity of the coastal bathymetry, with isolines aligned to the coastline, not influencing directly the occurrence of the coastal bulges, the orientation of coastline and the hydrodynamic effect of winds along the delta boundaries can trigger and increase the spatial and temporal variability of the occurrence of the studied features.

One aspect that arises from the modelling results for two events, one in extreme flood and the other in moderate flood conditions, is that the presence of marine water bulges can be detected in both cases, suggesting that, even if the amount of freshwater from the river is able to modulate the process, it is not sufficient to affect its occurrence. Moreover, considering the range of cases analysed by SST images, warmer water bulges can be detected both in high (e.g. the 18th-19th of November 2014) and low discharge conditions (e.g. the 4th of December 2017). However, the different morphology of the branches can affect the spatial occurrence of marine water bulges near the coast. In the specific context of the Po River delta, the southern branches have similar characteristics in terms of width, depth and discharge. As shown in Maicu et al., 2018, the discharge rates of the southern branches vary in the range 14-16% of the total river outflow. On the other hand, it has to be mentioned that Po di Tolle and Po di Gnocca branches flow to the sea through three and two mouths, respectively (Fig. 1). Moreover, the load of water from the different branches does not keep the same ratio in low flood and in high flood conditions, leading to slightly different multiple discharge configurations (Nelson 1970, Maicu et al.,2018). Thermohaline characteristics are similar at each branch but their different amount of water, although limited, could be a source of asymmetry, acting differently on stratification, and spatial and temporal variability of bulge occurrence.

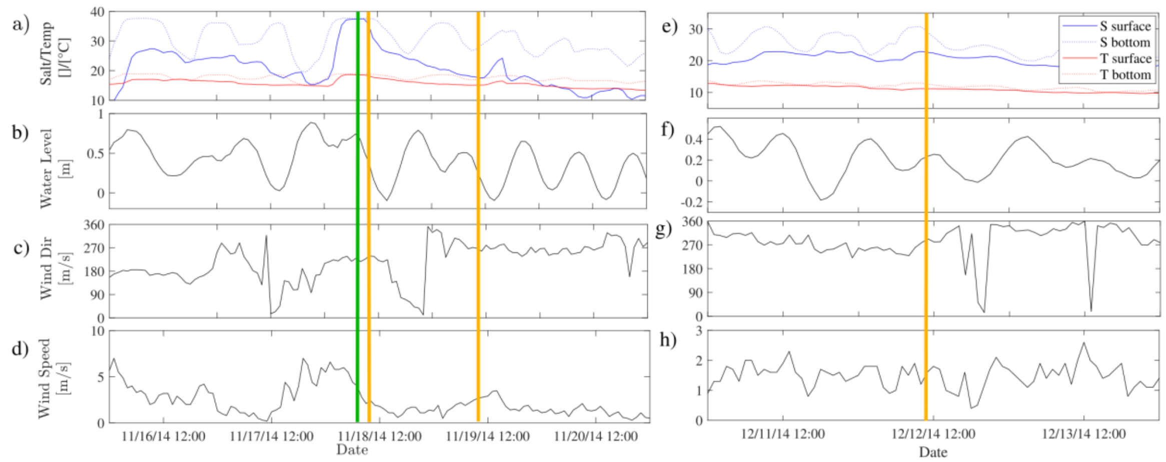

Figure 9: a,e) Surface (solid line) and bottom (dotted line) temperature (red) and salinity (blue); b,f) water level c,g) wind direction; d,h) wind speed timeseries extracted in one modelled point along the cross shore transects (black and yellow lines in Fig. 1, respectively) analised during and in the days preceeding the events of the 18th-19th November and 12th December 2014 (left and right panels). Orange lines represent the Landat 7 and Lansat 8 overpasses, the green line represents the moment of maximum upwelling recorded by the model.

Fig. 9 considers the simulated periods and shows the behaviour of modelled surface and bottom temperature and salinity south of the Pila mouth, where the warmer bulge appears (panel a), and it is clear how, after a more mixed condition during upwelling (18th of November, 9 UTC, green line), the tendency of the water column is to re-establish stratification. Moreover, Fig. 9d shows how there is a decrease in wind speed, suggesting a possible major effect, after upwelling due to wind, linked with tidal forcing and eventual residual seiches (Fig. 9b).
It is probable that what is experimentally detected on the 19th of November 2014 is a residual signal of the already occurred upwelling, in the process for re-stratification in absence of major driving winds. Similarly, the 12th of December 2014 shows a configuration not mainly driven by the wind, but more likely by the combination of wind and tidal action.

To clarify the wind effects on the occurred upwelling, salinity and temperature cross-shore transects for the ALL, NOTIDE and NOWIND runs, also for the 18th of November, 9 UTC (maximum upwelling detected from model), are discussed (Fig. 10).

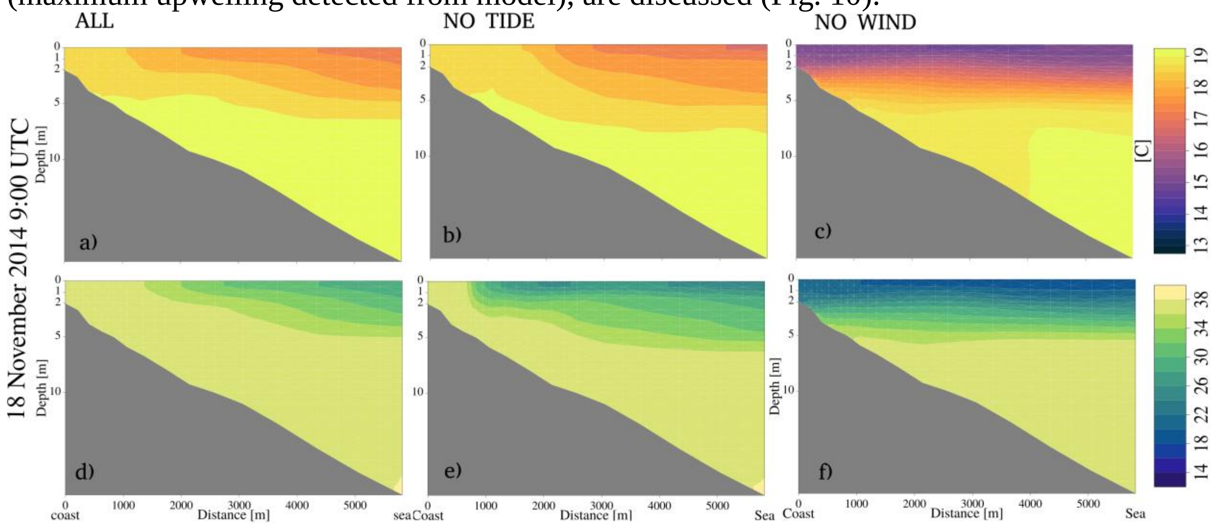

Figure 10: Temperature (a,b,c panels) and salinity (d,e,f panels) transects in the study area (black line in Fig.1) for the three simulations on the 18th of November 2014, 9:00 UTC.

ALL run transects evidenced that on the 18th of November the coastal bulge was in correspondence with an upwelling point, with well mixed temperature (18°C, Fig. 10a) and salinity (around 37, Fig. 10d). Excluding the tidal forcing allows the wind blowing to enhance the upwelling (larger coastal band with well mixed waters at 18°C, Fig. 10, b). On the other hand, the absence of wind forcing leads to a stratified water column, both in salinity and temperature, opposing possible upwelling. On the 18^{th} of November, the wind was blowing from SW with a speed of about 4 ms^{-1} (the wind speed was even higher in the hours before the satellite overpass, up to 7 ms^{-1} , same direction, Fig. 9c and d). As well described in the review from Lentz and Fewings (2012), winds blowing over a stratified water column produce an inner shelf region unstratified or weakly stratified and a middle shelf outer zone well stratified (Fig. 10 a and d). Asymmetric responses, in terms of vertical and cross-shelf patterns in the upwelling and downwelling favourable cases, respectively. In downwelling favourable cases the inner shelf tends to be unstratified because continuously fed by the surface waters flowing inshore. Upwelling favourable winds, on the other hand, generally produce just a less stratified inner shelf area and cross-shelf currents onshore of the upwelling zone are not totally damped, as in the case of downwelling (Lentz and Fewings, 2012). This latter is the situation that can be detected on the 18^{th} of November 2014 and shown in temperature and salinity when just wind is acting (Fig. 10 b and e).

To verify the effect of wind forcing, we can consider evidences from Fig. 11 that shows the predominant term of the momentum equation in a certain area, simultaneously to the satellite overpasses: in fact, for the 18^{th} of November the warmer bulge area is characterised by the wind stress term (green zone).

Moreover, considering the 12^{th} of December event, Fig. 11c proves how in correspondence of the larger warmer and saltier water bulge just south of Pila mouth and in front of Po di Tolle river branch (Fig.2c) the system seems less dynamic at the surface. A large area where there is not the prevailing contribution of wind stress, baroclinic pressure gradients or advection is detected.

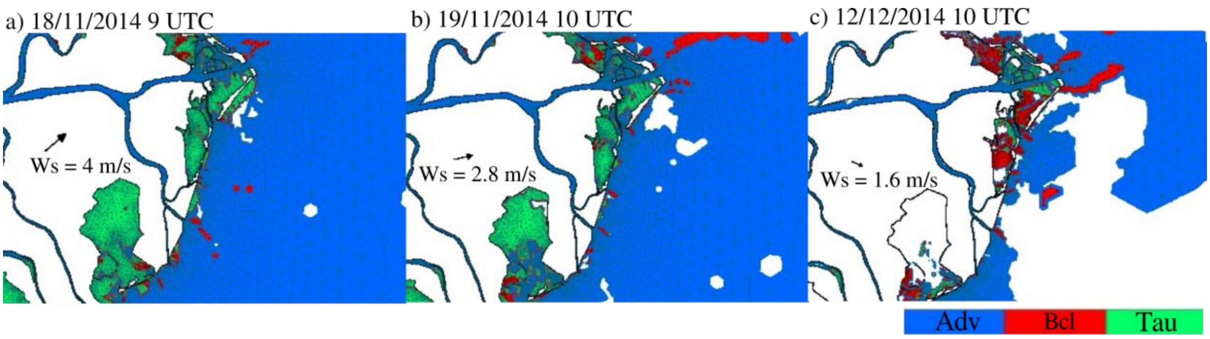

Figure 11: Thematic surface maps representing the prevailing term of momentum equation between the horizontal advective (blue - Adv), the baroclinic pressure gradient (red - Bcl) and the wind surface stress (green - Tau), for the 18^{th} of November 2014, 9:00 UTC, the 19^{th} of November 2014, 10:00 UTC and the 12^{th} of December 2014, 10:00 UTC. White areas are where the relative contribution of each term is below a threshold, therefore considering that the area is less dynamic.

As suggested by Figs. 6, 7 and 8, tides are not the driving forcing, but they can modulate and affect the occurrence of warmer water bulges occurrence. The interaction between stratified waters, as those belonging to river plumes, and tidal forces is described in the tidal straining theory (Simpson et al., 1990) and evidences are shown in Simpson and Souza (1995) and De Boer et al. (2009). Simpson et al. (1993) noted how, for the river Rhine ROFI, spring tides combined with winds tend to produce well-mixed plumes, while neap tides lead to stratified plumes. Applying this evidence to the considered plumes and noting that both the 19^{th} of November 2014 and the 12^{th} of December 2014 are close to neap tide phase, we would expect a more stratified water column. Moreover, from Simpson and Souza (1995) we know that the short-term variability, due to semidiurnal tidal signal, interacts with baroclinic gradients producing vertical variations in stability of the water column. Particularly, in stratified waters there is a decoupling between the surface and the bottom tidal currents (increased anticyclonic and cyclonic tendency above and below the pycnocline, respectively, due to the higher effects of bottom friction on the tidal component opposed to earth rotation – Souza and Simpson 1996; De Boer et al. 2009), producing cross-shore currents. The presence of the coastal boundary, for continuity, forces the system to compensate the two-way horizontal water mass movement with possible up- or downwelling.

The warmer and saltier waters are modulated, on a periodicity of 12 hours as expected from tidal straining theory, in the sequence upwelling-lateral deflection-downwelling-opposite lateral deflection.

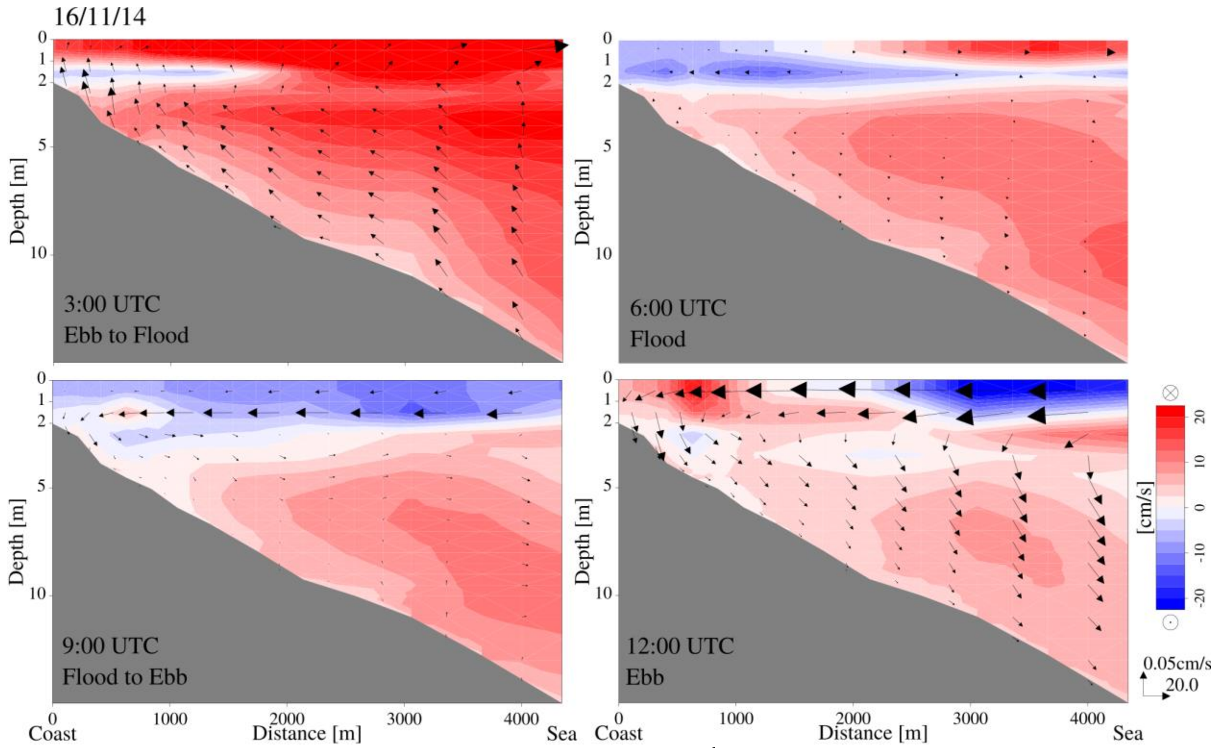

Figure 12: Velocity transects (black line in Fig. 1) of the day 16th of November 2014, corresponding to Ebb to Flood (3 UTC), Flood (6 UTC), Flood to Ebb (9 UTC), Ebb (12 UTC) tidal phase. Colours correspond to normal velocity.

The Fig. 12, on the 16th of November, shows this sequence in a period of weak wind, resulting in a clearer detection of the effect of the tidal phase. At 3:00 UTC the tide in ebb to flood phase and the velocity transect shows a clear upwelling, with a general coastal current to north (Fig. 12a); three hours later, in full flood phase, as tidal straining theory predicts, the surface current flows to south, up to 3 m depth, with a decrease in intensity and inversion of direction offshore (Fig. 12b). In flood to ebb phase the velocities normal to the coast show downwelling, with the surface current flowing to south and bottom currents to north, probably evidence of the decoupling above and below pycnocline with anticyclonic and cyclonic tendency, respectively (Fig. 12c). Finally, in ebb phase, at 12 UTC, coastal current flows to north (Fig. 12d).

Evidences of different phases of tidal straining can be detected also on the two cases discussed in the results, on the 19th of November 2014 and on the 12th of December 2014.

In the former case the system is in the flood to ebb phase and we know that this facilitates coastal downwelling in stratified waters, therefore tides work, for this event, against the detected process. The 19th of November 2014 seems more a residual signal of the process occurred the day before. This is confirmed by the results shown in Fig. 11: the area corresponding to the warmer bulge south of Pila mouth, where the 18^{th} of November wind stress term was the major contribution, shows now the predominance of the advective term.

For the event of the 12^{th} of December 2014, the tidal phase was from ebb to flood and wind was around 2 ms^{-1} from W S-W (Fig. 9 g, h). According to the tidal straining theory, the ebb to flood phase is contributing to coastal upwelling. There are confirmations of this tendency in Fig. 8, but just in temperature and at the bottom. Also, the tidal signal for this event is weaker than on the previous events (water level range 30 vs. $70 - 90$ cm). Even if quite weak, in this case winds are mainly aligning to the southern side of the delta coast, from the direction W-SW, therefore the wind configuration seems to follow the Ekman theory on upwelling. In such conditions, with limited energy due to tides and winds, despite the identified mechanisms should enhance upwelling, they have detectable effects limited to portions of the water column (wind in the very surface, tidal straining at the bottom) and they do not allow the full development of the vertical phenomenon. Also, the area where the warmer bulge is observed seems horizontally weakly dynamic, as confirmed by Fig. 11.

The event of the 12^{th} of December 2014 shows also how water from the bulges can transitorily spread into the delta lagoons (i.e. Caleri, Fig. 7a), modifying their thermohaline characteristics, eventually producing effects on lagoons' hydrology and ecosystems. Finally, this case is an example of how the appearance of coastal marine bulges can occur also when river-sea temperature gradients are small. This aspect suggests that the lateral thermal gradient on the surface does not play a significant role in driving this process.

So far, all the discussed cases where identified in late fall or winter seasons. We hypothesised that their detection from satellite, mainly based on the evidence in temperature from SST maps, could bias our interpretation on the actual occurrence of these phenomena, considering that they are less evident from earth observation (EO) data in other seasons, just due to the lower difference in temperature between river and sea waters. Therefore, we considered modelled data from a two year run (2010-2011) whose data are discussed in Maicu et al. 2018. Two timeseries were extracted from a set of two points, one north and one south of the Pila mouth, where generally the warmer water bulges are seen (Fig. 1, white stars).

First, we evaluated the timeseries of the surface-bottom salinity difference, performing the Fast Fourier Transform (FFT) analysis to identify possible short scale periodic signals on the vertical salinity stratification. As expected and evident from Fig. 13, two peaks are seen, corresponding to 6 and 12 hour periods: upwelling and downwelling induced by tidal straining are homogenizing the water column every 6 hours.

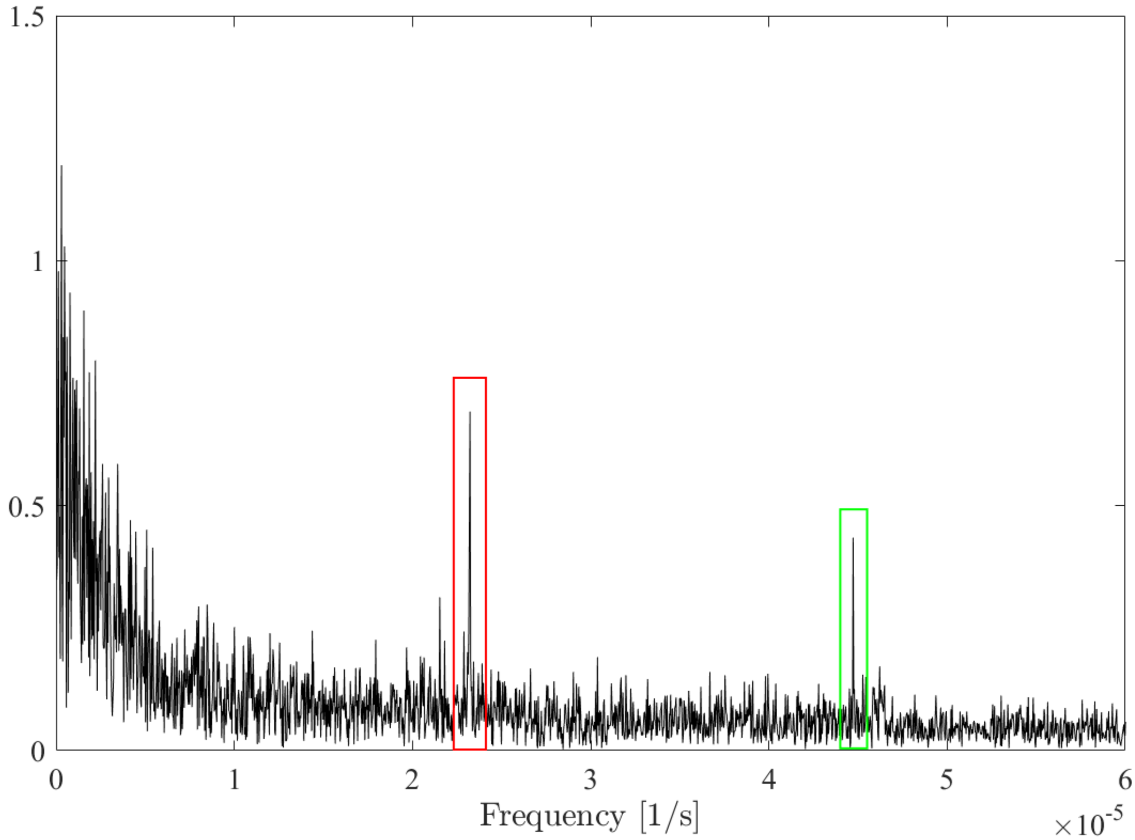

Figure 13: Fast Fourier Transform for the timeseries extracted in one point south of the Pila mouth (white star in Fig. 1), spanning the years 2010 and 2011 of bottom-surface salinity difference. Red box corresponds to the semi-period signal of K1 tidal component, green box to the one of M2 tidal component.

Then we performed a seasonal analysis of the occurrence of the studied water bulges, arbitrarily identified by the records when the surface-bottom salinity difference is lower than 4, with surface salinity values > 30. The number of these cases covers the 9.8% and the 14.4% of total records in the points north and south of the Pila mouth, respectively. The larger number of cases occurs in winter (3.6%, compared to spring, summer and fall - 2.9%, 1.5%, 1.8%) in the southern coast of the Po Delta; in spring (4.9%, compared to winter, summer and fall - 3.3%, 2.9%, 3.3%) in the northern coast.

Corresponding to the seasonal events identified, wind roses where produced, considering the 12 hours interval preceding each case, and providing indication on characteristic wind regimes, as well as possible explanation of the seasonal occurrence of the phenomenon. For the point extracted north of the Pila mouth, where the coast is oriented NW-SE, it is evident that on spring, summer and fall there is a major regime blowing from SE that aligns to the coast and can potentially determine upwelling (Fig. 14, upper panels).

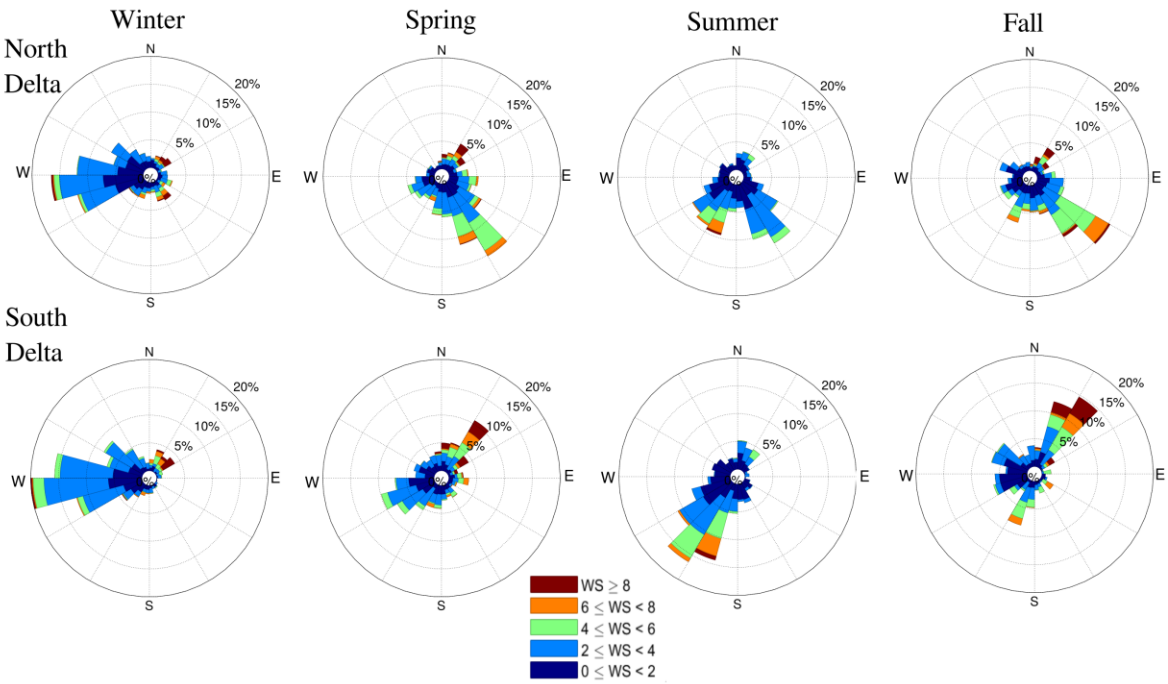

Figure 14: Wind roses representing the seasonal distribution of wind events occurring simultaneously to the cases when water column is homogeneously mixed in salinity, with salinity values higher than 30 in two points (white stars in Fig. 1) located north and south of the Pila mouth (top and bottom panels, respectively).

Moreover, the winter distribution show a majority of winds blowing from SW, therefore from land to sea. On the coast south of the Pila mouth, directed SW-NE, winter cases are, as above, characterized by land to sea winds, while spring also shows intense Bora winds (> 8 ms^{-1}) that are, in these area, downwelling favourable. Summer shows a predominance of upwelling-favourable cases, with winds from SW. Finally, the fall shows two major regimes, with high speed winds, one from SW and the other from NE, upwelling and downwelling favourable along that coast, respectively (Fig. 14, lower panels). As was also evident in the cases discussed in this paper, the fall seems to alternate upwelling and downwelling.

5. Conclusion

The present work aimed at investigating the mixing processes that originate and drive the dynamics of coastal small scale warmer and saltier water bulges, visible between river mouths. The present study moved from the interest in the identification of the interaction processes between river inputs and sea waters, investigating aspects that can be found in a number of river-sea systems, not only in our study area, the Po River Delta.

The integration of satellite-derived products, in situ measurements and modelling results was the tool and the added value to perform both the 3D investigation of the phenomena and their temporal evolution.

The simulated cases showed how tides and winds, blowing from land and along the southern coast of the Po River Delta, are responsible for localized upwelling process, leading to the formation of the warmer saltier water bulges close to the coast, previously described with fine scale SST maps by Brando et al. (2015). Vertical mixing takes place, homogenizing the water column and permitting the identification of warmer, saltier waters in specific coastal spots.

These localized events interact with the advective forces connected to the outflow of the different river branches.

The river discharge magnitude, even if does not seem to be the main driver of the process, contributes to the definition of the stratification of surrounding waters injected into the system

by the buoyant plume, therefore enhancing or weakening the action of tidal straining in the very coastal area.
Tidal forcing in ebb to flood phase strengthen the process and a semidiurnal modulation can be seen.
However, not all the cases when warmer bulges are detected from satellite products correspond to fully developed upwelling, even if the mechanisms leading to upwelling surely contribute in enhancing the bulges evidence.
The analysis of modelled timeseries showed that the occurrence of these warmer saltier bulges is not limited to one season. The southern coast of the delta shows the highest number of cases in winter, generally in correspondence to upwelling favourable winds, and significant cases in the other seasons. In particular, during the fall season there is the alternation of up and downwelling favourable wind conditions. On the northern area, the highest occurrence is in spring, when upwelling favourable winds occur.
Despite none of the main wind regimes that characterize the area (Bora from north-east and Sirocco from south-east) are acting, weak wind events blowing from land and aligning to the coast were found to have an effect on determining the coastal hydrodynamics and thermohaline characteristics of the very coastal waters.
The joint action of the identified forcing allow the presence of warmer saltier waters also close to the Po River Delta lagoons, temporarily modifying the thermohaline characteristics of these sub-systems. These warm and saltier bulges can affect the coastal system hydrology, ecological features and, eventually, the vertical dynamics can affect coastal mixing and sediment dynamics.

Acknowledgments

The authors wish to thank Consorzio di Bonifica Deltapo for providing bathymetry data of Po Delta lagoons, AIPO (Agenzia Interregionale per il fiume Po) for the internal river branches bathymetry, the Regional Environmental Protection Agency of Emilia-Romagna (ARPAE) for providing Goro lagoon bathymetry and the Po river discharges and temperature, the Regional Environmental Protection Agency of Veneto (ARPAV) for meteorological data from Po di Tolle monitoring station and Adige river discharges. Landsat 8 and Landsat 7 data are available from the U.S. Geological Survey. This research was partially funded by the Flagship Project RITMARE – The Italian Research for the Sea coordinated by the Italian National Research Council and funded by the Italian Ministry of Education, University and Research. The work was also undertaken as part of the costeLAB Project (Progetto Premiale ”Rischi Naturali Indotti dale Attivitá Umana - COSTE”, CIG 6256318CED), funded by the Italian Space Agency and the CoastObs project (H2020, project number 776348). This study was inspired by the activities of the scientific community that is building the ESFRI DANUBIUS Research Infrastructure, the International Centre for Advanced Studies on River-Sea Systems (http://www.danubiusri.eu/).

References

Androulidakis Y.S., Kourafalou V.H. and Schiller R.V. Process studies on the evolution of the Mississippi River plume: Impact of topography, wind and discharge conditions Continental Shelf Research, 107, 33–49, 2015.

Artegiani, A., Paschini, E., Russo, A., Bregant, D., Raicich, F., Pinardi, N., 1997a. The Adriatic Sea general circulation. Part I: air-sea interactions and water mass structure. Journal of Physical Oceanogry 27 (8), 1492–1514. https://doi.org/10.1175/1520-0485(1997) 0271492:TASGCP2.0.CO;2.

Artegiani, A., Paschini, E., Russo, A., Bregant, D., Raicich, F., Pinardi, N., 1997b. The Adriatic Sea general circulation. Part II: baroclinic circulation structure. Journal of Physical Oceanogry 27 (8), 1515–1532. https://doi.org/10.1175/15200485(1997) 0271515:TASGCP2.0.CO;2.

Barsi, J.A., Schott, J.R., Palluconi, F.D. and Hook, S.J. Validation of a web-based atmospheric correction tool for single thermal band instruments. Opt. Photon.,(58820E), 1-7, 2005.

Barsi, J., Schott, J., Hook, S., Raqueno, N., Markham, B., & Radocinski, R. (2014). Landsat-8 thermal infrared sensor (TIRS) vicarious radiometric calibration. *Remote Sensing*, *6*(11), 11607-11626.

Bellafiore, D. & Umgiesser, G. Hydrodynamic coastal processes in the North Adriatic investigated with a 3D finite element model. Ocean Dyn. 60, 255-273, 2010.

Bellafiore, D., McKiver, W.J., Ferrarin, C. and Umgiesser, G. The importance of modeling nonhydrostatic processes for dense water reproduction in the Southern Adriatic Sea Ocean Modelling 125, 22-38, 2018.

Boldrin, A., Langone, L., Miserocchi, S., Turchetto, M. and Acri, F. Po River plume on the Adriatic continental shelf: dispersion and sedimentation of dissolved and suspended matter during different river discharge rates. Marine Geology,222,135–158, 2005. http://dx.doi.org/10.1016/j.margeo.2005.06.010.

Brando, V.E., Braga, F., Zaggia, L., Giardino, C., Bresciani, M., Matta, E., Bellafiore, D., Ferrarin, C., Maicu, F., Benetazzo, A., Bonaldo, D., Falcieri, F.M., Coluccelli, A., Russo, A. and Carniel, S. High-resolution satellite turbidity and sea surface temperature observations of river plume interactions during a significant flood event. Ocean Sci., 11, 909-920, 2015. https://doi.org/10.5194/os-11909-2015.

Braga, F., Zaggia, L., Bellafiore, D., Bresciani, M., Giardino, C., Lorenzetti, G.,Maicu, F. Manzo, C., Riminucci, F., Ravaioli, M. and Brando, V. E Mapping turbidity patterns in the Po river prodelta using multi-temporal Landsat 8 imagery. Estuarine, Coastal and Shelf Science, 198, 555-567.

Chant, R. J., Glenn, S. M., Hunter, E., Kohut, J., Chen, R. F., Houghton, R. W., ... & Schofield, O. (2008). Bulge formation of a buoyant river outflow. Journal of Geophysical Research: Oceans, 113(C1).

Cole, K. L., & Hetland, R. D. (2016). The effects of rotation and river discharge on net mixing in small-mouth Kelvin number plumes. Journal of Physical Oceanography, 46(5), 1421-1436.

Davis, K. A., N. S. Banas, S. N. Giddings, S. A. Siedlecki, P. MacCready, E. J. Lessard, R. M. Kudela, and B. M. Hickey Estuary-enhanced upwelling of marine nutrients fuels coastal productivity in the U.S. Pacific Northwest. Journal of Geophysical Research -Oceans,119, 8778–8799, 2014. doi:10.1002/2014JC010248.

de Boer, G.J., Pietrzak, J. and Winterwerp, J.C. SST observations of upwelling induced by tidal straining in the Rhine ROFI Continental Shelf Research, 29, 263–277, 2009. Doi:10.1016/j.csr.2007.06.011

Donlon, C. J., Minnett, P. J., Gentemann, C., Nightingale, T. J., Barton, I. J., Ward, B., and Murray, M. J. Toward improved validation of satellite sea surface skin temperature measurements for climate research. Journal of Climate, 15(4), 353-369, 2002.

Fairall, C.W., Bradley, E.F., Hare, J.E., Grachev, A.A. and Edson, J.B. Bulk Parameterization of Air-Sea Fluxes: Updates and Verification for the COARE Algorithm. J Climate,16(4),571–591, 2003.

Falcieri, F.M., Benetazzo, A., Sclavo, M., Russo, A. and Carniel, S. Po River plume pattern variability investigated from model data Continental Shelf Research, 87,84–95, doi:10.1016/j.csr.2013.11.001, 2014

Ferrarin, C., Maicu, F. and Umgiesser, G. The effect of lagoons on Adriatic Sea tidal dynamics. Ocean Modelling,119, 57–71, 2017.

Ferrarin, C., Davolio, S., Bellafiore, D., Ghezzo, M., Maicu, F., Mc Kiver, W., Drofa, O., Umgiesser, G., Bajo, M., De Pascalis, F., Malguzzi, P., Zaggia, L., Lorenzetti, G. and Giorgia Manfé Cross-scale operational oceanography in the Adriatic Sea Submitted to Journal of Operational Oceanopraphy, 2019.

Fong, D. A., & Geyer, W. R. (2002). The alongshore transport of freshwater in a surface-trapped river plume. Journal of Physical Oceanography, 32(3), 957-972.

Garvine, R.W. A dynamical system for classifying buoyant coastal discharges Continental Shelf Research, 15, 13, 1585–1596, 1995.

Hansen, D.V. and M. Jr. Rattray New Dimensions in Estuary Classification Limnology and Oceanography, 11,3,319–326,doi:10.4319/lo.1966.11.3.0319, 1966.

Hetland, R. D. (2005). Relating river plume structure to vertical mixing. Journal of Physical Oceanography, 35(9), 1667-1688.

Horner-Devine,A.R., Hetland, R.D. and MacDonald, D.G. Mixing and Transport in Coastal River Plumes Annual Review of Fluid Mechanics, 45,569–594, doi:10.1146/annurev-fluid-010313-141408, 2015.

Karstner, S.E., Horner-Devine, A.R. and Thomson, J. The influence of wind and waves on spreading and mixing in the Fraser River plume Journal of Geophysical Research - Ocean, ,–,2018. https://doi.org/10.1029/2018JC013765

Irons, J.R., Dwyer, J.L. and Barsi, J.A. The next Landsat satellite: the Landsat data continuity mission. Remote Sens. Environ.,122, 11–21. http://dx.doi.org/10.1016/j.rse.2011.08.026.

Isobe, A. (2005). Ballooning of river-plume bulge and its stabilization by tidal currents. Journal of Physical Oceanography, 35(12), 2337-2351.

Lentz, S.J., Fewings, M.R., 2012. The wind- and wave-driven inner-shelf circulation. Ann. Rev. Mar. Sci. 4 (1), 317–343. https://doi.org/10.1146/annurev-marine-120709-142745.

Leonardi, N., A. Canestrelli, T. Sun, and S. Fagherazzi (2013), Effect of tides on mouth bar morphology and hydrodynamics, J. Geophys. Res. Oceans, 118, 4169–4183, doi:10.1002/jgrc.20302.

Leonardi, N., Kolker, A. S., & Fagherazzi, S. (2015). Interplay between river discharge and tides in a delta distributary. Advances in water resources, 80, 69-78.

Longdill, P.C., Healy, T.R. and Black, K.P. Transient wind-driven coastal upwelling on a shelf with varying width and orientation New Zealand Journal of Marine and Freshwater Research, 42,2,181–196, 2008. Doi: 10.1080/00288330809509947.

Maicu, F., De Pascalis, F., Ferrarin, C., and Umgiesser, G. Hydrodynamics of the Po River-Delta-Sea system. Journal of Geophysical Research: Oceans, 123, 2018. Doi: https://doi.org/10.1029/2017JC013601

Manzo, C., Braga, F., Zaggia, L., Brando, V.E., Giardino, C., Bresciani, M., Bassani, C., 2018. Spatio-temporal analysis of prodelta dynamics by means of new satellite generation: the case of Po river by Landsat-8 data. Int. J. Appl. Earth Obs. Geoinf. 66, 210–225.

Mariotti, G., Falcini, F., Geleynse, N., Guala, M., Sun, T., & Fagherazzi, S. (2013). Sediment eddy diffusivity in meandering turbulent jets: Implications for levee formation at river mouths. Journal of Geophysical Research: Earth Surface, 118(3), 1908-1920.

Martí-Cardona, B., Prats, J., & Niclòs, R. (2019). Enhancing the retrieval of stream surface temperature from Landsat data. *Remote Sensing of Environment*, *224*, 182-191.

Maselli, V., & Trincardi, F. (2013). Man made deltas. *Scientific Reports*, *3*, [1926]. DOI: 10.1038/srep01926

Nelson, B.W. Hydrography, sediment dispersal, and recent historical development of the Po River Delta in Deltaic Sedimentation: Modern and Ancient,editor J.P. Morgan, Soc. Econ. Paleontologists and Mineralogists, New York,152–184,1970.

O’Donnell, J. The dynamics of estuary plumes and fronts, chapter in Book ”Contemporary Issues in Estuarine Physics” , editor A. Valle-Levinson, Cambridge, 186–246, 2010.

Orlić, M., Kuzmić, M. and Pasarić, Z. Response of the adriatic sea to the Bora and Sirocco forcing. Continental Shelf Research,14 (1), 91–116, 1994. http://dx.doi.org/10.1016/0278-4343(94)90007-8.

Polli, S. La propagazione delle maree nell’Adriatico. Atti X Convegno Associazione Geofisica Italiana, 1–11,1960.

Simpson, J.H., Brown, J., Matthews, J. and Allen, G. Tidal straining,density currents, and stirring in the control of estuarine stratification Estuaries, 13(2), 125–132,1990.

Simpson, J.H., Bos, W.G., Schirmer, F., Souza, A.J., Rippeth, T.P., Jones, S.E. and Hydes, D.

Periodic Stratification in the Rhine ROFI in the North Sea Oceanologica Acta, 16(1), 23–32, 1993.

Simpson, J.H. and Souza, A. Semidiurnal switching of stratification in the region of freshwater influence of the Rhine. Journal of Geophysical Research, 100(C4), 7037–7044, 1995.

Souza, A. and Simpson, J.H. The modification of tidal ellipses by stratification in the Rhine ROFI Continental Shelf Research,16 (8),997–1007, 1996.

Tesi, T., Miserocchi, S., Goni, M.A., Turchetto, M., Langone, L., De Lazzari, A., Albertazzi, S. and Correggiari, A. Influence of distributary channels on sediment and organic matter supply in event-dominated coastal margins: the Po prodelta as a study case Biogeosciences,8,365–385,2011.

Umgiesser, G., Ferrarin, C., Cucco, A., De Pascalis, F., Bellafiore, D., Ghezzo, M. and Bajo, M. Comparative hydrodynamics of 10 Mediterranean lagoons by means of numerical modeling Journal of Geophysical Research, 119(4), 2212–2226, 2014, doi:https://doi.org/10.1002/2013JC009512

Umgiesser, G., Ferrarin, C., Fivan, Bajo, M., 2018. SHYFEM-model/shyfem: Stable release 7.4.1 (Version VERS_7_4_1). Zenodo. http://doi.org/10.5281/zenodo.1311751.

Zavatarelli, M., Pinardi, N., Kourafalou, V.H. and Maggiore, A. Diagnostic and prognostic model studies of the Adriatic Sea general circulation: seasonal variability. Journal of Geophysical Research-Oceans, 107 (C1), 2002. http://dx.doi.org/10.1029/2000JC000210.

Warrick, J.A., Farnsworth, K.L Coastal river plumes: Collisions and coalescence Progress in Oceanography,151,245–260, 2017.

Wiseman, J.W. and Garvine, R.W. Plumes and Coastal Large River Mouths Estuaries,18(3), 509–517, 1995.

Yuan, Y., Horner-Devine, A.R. Laboratory investigation of the impact of lateral spreading on buoyancy flux in a river plume Journal of Physical Oceangraphy,43(2), 588–610, 2011.